Lawrence Berkeley National Laboratory
LBL Publications

Title
Multiple Viral microRNAs Regulate Interferon Release and Signaling Early during Infection with Epstein-Barr Virus.

Permalink
https://escholarship.org/uc/item/2kk1b64f

Journal
mBio, 12(2)

ISSN
2150-7511

Authors
Bouvet, Mickaël
Voigt, Stefanie
Tagawa, Takanobu
et al.

Publication Date
2021-03-30

DOI
10.1128/mbio.03440-20

Copyright Information
This work is made available under the terms of a Creative Commons Attribution License, available at https://creativecommons.org/licenses/by/4.0/

Peer reviewed

eScholarship.org Powered by the California Digital Library
University of California

AMERICAN SOCIETY FOR MICROBIOLOGY | mBio®

RESEARCH ARTICLE

Multiple Viral microRNAs Regulate Interferon Release and Signaling Early during Infection with Epstein-Barr Virus

Mickaël Bouvet,[a] Stefanie Voigt,[a] Takanobu Tagawa,[a]* Manuel Albanese,[a] Yen-Fu Adam Chen,[a] Yan Chen,[b] Devin N. Fachko,[b] Dagmar Pich,[a] Christine Göbel,[a] Rebecca L. Skalsky,[b] Wolfgang Hammerschmidt[a]

[a]Research Unit Gene Vectors, Helmholtz Zentrum München, German Research Center for Environmental Health and German Center for Infection Research (DZIF), Partner site Munich, Munich, Germany

[b]Vaccine and Gene Therapy Institute, Oregon Health & Science University, Beaverton, Oregon, USA

ABSTRACT Epstein-Barr virus (EBV), a human herpesvirus, encodes 44 microRNAs (miRNAs), which regulate many genes with various functions in EBV-infected cells. Multiple target genes of the EBV miRNAs have been identified, some of which play important roles in adaptive antiviral immune responses. Using EBV mutant derivatives, we identified additional roles of viral miRNAs in governing versatile type I interferon (IFN) responses upon infection of human primary mature B cells. We also found that Epstein-Barr virus-encoded small RNAs (EBERs) and LF2, viral genes with previously reported functions in inducing or regulating IFN-I pathways, had negligible or even contrary effects on secreted IFN-α in our model. Data mining and Ago PAR-CLIP experiments uncovered more than a dozen previously uncharacterized, direct cellular targets of EBV miRNA associated with type I IFN pathways. We also identified indirect targets of EBV miRNAs in B cells, such as TRL7 and TLR9, in the prelatent phase of infection. The presence of epigenetically naive, non-CpG methylated viral DNA was essential to induce IFN-α secretion during EBV infection in a TLR9-dependent manner. In a newly established fusion assay, we verified that EBV virions enter a subset of plasmacytoid dendritic cells (pDCs) and determined that these infected pDCs are the primary producers of IFN-α in EBV-infected peripheral blood mononuclear cells. Our findings document that many EBV-encoded miRNAs regulate type I IFN response in newly EBV infected primary human B cells in the prelatent phase of infection and dampen the acute release of IFN-α in pDCs upon their encounter with EBV.

IMPORTANCE Acute antiviral functions of all nucleated cells rely on type I interferon (IFN-I) pathways triggered upon viral infection. Host responses encompass the sensing of incoming viruses, the activation of specific transcription factors that induce the transcription of IFN-I genes, the secretion of different IFN-I types and their recognition by the heterodimeric IFN-α/β receptor, the subsequent activation of JAK/STAT signaling pathways, and, finally, the transcription of many IFN-stimulated genes (ISGs). In sum, these cellular functions establish a so-called antiviral state in infected and neighboring cells. To counteract these cellular defense mechanisms, viruses have evolved diverse strategies and encode gene products that target antiviral responses. Among such immune-evasive factors are viral microRNAs (miRNAs) that can interfere with host gene expression. We discovered that multiple miRNAs of Epstein-Barr virus (EBV) control over a dozen cellular genes that contribute to the antiviral states of immune cells, specifically B cells and plasmacytoid dendritic cells (pDCs). We identified the viral DNA genome as the activator of IFN-α and question the role of abundant EBV EBERs, that, contrary to previous reports, do not have an apparent inducing function in the IFN-I pathway early after infection.

KEYWORDS B cells, Epstein-Barr virus, immune evasion, interferons, microRNA, plasmacytoid dendritic cells

Citation Bouvet M, Voigt S, Tagawa T, Albanese M, Chen Y-FA, Chen Y, Fachko DN, Pich D, Göbel C, Skalsky RL, Hammerschmidt W. 2021. Multiple viral microRNAs regulate interferon release and signaling early during infection with Epstein-Barr virus. mBio 12: e03440-20. https://doi.org/10.1128/mBio.03440-20.

Editor Matthew S. Miller, McMaster University

Copyright © 2021 Bouvet et al. This is an open-access article distributed under the terms of the Creative Commons Attribution 4.0 International license.

Address correspondence to Wolfgang Hammerschmidt, hammerschmidt@helmholtz-muenchen.de.

* Present address: Takanobu Tagawa, HIV and AIDS Malignancy Branch, Center for Cancer Research, National Cancer Institute, National Institutes of Health, Bethesda, Maryland, USA.

Received 4 December 2020
Accepted 18 February 2021
Published 30 March 2021

Epstein-Barr virus (EBV) is a DNA virus of the gammaherpesvirus family that establishes persistent, lifelong infection in the majority of the worldwide human population. Despite being mostly asymptomatic, EBV infection can cause infectious mononucleosis and lead to severe diseases, such as Burkitt lymphoma (BL), diffuse large B cell lymphoma (DLBCL), nasopharyngeal carcinoma, and posttransplant lymphoproliferative disease (PTLD). PTLD and HIV-associated DLBCL develop in immunosuppressed and immunocompromised individuals, highlighting the ability of the human immune system to keep EBV infection under control but the inability to reach total viral clearance.

EBV achieves latency in B lymphocytes through different phases, which are characterized by the expression and downregulation of multiple viral gene products, ultimately decreasing the antigenic load of infected cells. EBV preferentially infects B lymphocytes and can even readily transform primary B lymphocytes into an indefinitely proliferating lymphoblastoid cell line (LCL) *in vitro*. Additional cell types in the blood, including plasmacytoid dendritic cells (pDCs), have been reported to express viral gene products upon contact with EBV virions but cannot be transformed *in vitro* (1 and references therein). Apart from viral proteins, the EBV genome carries different classes of noncoding RNAs, including two long noncoding RNAs, EBV small RNAs 1 and 2 (EBER1 and EBER2), circular RNAs (2), and 44 mature microRNAs (miRNAs) distributed in clusters along the genome (Fig. 1).

To conduct a successful infection, viruses, including EBV, must evade or counteract the activation of type I interferons (IFN-I). IFN-I production and signaling is a two-part system at the center of innate antiviral immunity. Initially, specialized pattern recognition receptors (PRRs) detect pathogen-associated molecular patterns (PAMPs), which are distinct pathogen structures otherwise absent from noninfected, healthy cells. PRR engagement triggers the activation of specific transcription factors that, in turn, induce transcription of IFN-I genes (13 IFN-α subtypes and IFN-β in humans), leading to production and secretion of type I IFNs. Secreted IFN-I binds to a single, heterodimeric IFN-α/β receptor on mammalian cells, thereby activating JAK/STAT signaling pathways and culminating in the transcription of many IFN-stimulated genes (ISGs). These gene products together establish a so-called antiviral state, thereby restricting the virus life cycle and/or orchestrating viral clearance in infected and neighboring cells.

Due to their peculiar faculty to secrete massive amounts of IFN-I, pDCs are a major factor in the IFN-I system. pDCs constitutively express major components of the IFN-I activation pathway, like the TLR7 and TLR9 PRRs and the interferon regulatory factor 7 (IRF7) transcription factor. TLR7 and TLR9 are embedded in the endosomal membranes and recognize single-stranded RNA (ssRNA) or unmethylated CpG DNA, respectively, in the endosomal lumen. Upon binding of PRRs, TLR7 and TLR9 signal through the MyD88 adaptor protein and activate the IRF7 transcription factor. There are hints that EBV is detected by pDCs, which respond to infection by secreting type I IFNs (3 to 6). Whether the virus infects human pDCs and the mechanisms by which pDCs detect EBV are not fully understood.

It has been shown that the EBERs, which are abundant viral noncoding RNAs, can be recognized as PAMPs by the RIG-I, TLR3, and TLR7 PRRs and that pDCs further sense the presence of EBV through recognition of unmethylated viral genomic DNA by TLR9 (3). Multiple intracellular sensors recognize exogenous cytosolic DNA, including DNA-dependent activator of IFN regulator factors (DAI) (7), DDX41 (8), absent in melanoma 2 (AIM2) (9), LSm14A (10), IFN-γ-inducible factor 16 (IFI16) (11), and cyclic GMP-AMP (cGAMP) synthase (cGAS) (12), which activates the adaptor protein STING (stimulator of IFN genes) to trigger IFN signaling. Human B cells express IFI16, cGAS, and downstream signaling components necessary to induce type I IFN; however, it has been demonstrated that B lymphocytes fail to recognize the presence of genomic EBV DNA through cGAS-STING (13).

EBV encodes several proteins that have been described as type I IFN antagonists and have been attributed roles in counteracting antiviral responses. In screening 150

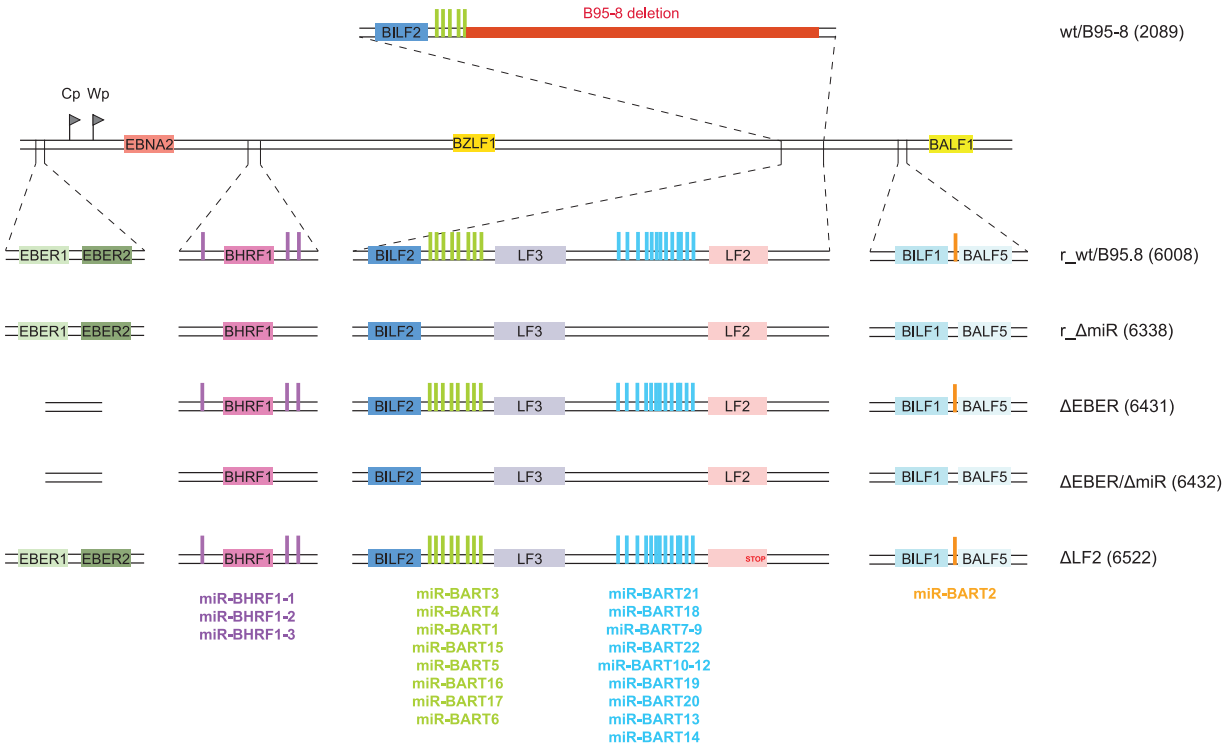

FIG 1 Construction of a reconstituted wild-type EBV genome and EBV mutants. An 11.8-kb fragment of the M-ABA strain complementing the deletion in EBV B95-8 was introduced by homologous recombination into wt/B95.8 (2089) to generate r_wt/B95.8 (6008) (for the reconstituted wild type). The 11.8-kb fragment contains the coding sequences of the LF2 and LF3 viral proteins and the majority of the BART miRNAs, allowing for expression of these viral miRNAs at physiological levels. EBV r_wt/B95.8 (6008) was mutated to eliminate expression of the viral miRNAs, the EBERs, or the LF2 protein. The r_ΔmiR (6338) strain was created by sequentially introducing three DNA fragments in which the viral pre-miRNA loci have been scrambled to prevent the formation of the characteristic hairpin structure recognized and processed by the ribonucleases Drosha and Dicer to generate mature miRNAs. The ΔEBER (6431) and ΔEBERΔmiR (6432) strains were created by insertional mutagenesis deleting the EBERs coding genes in r_wt/B95.8 and r_ΔmiR EBV derivatives, respectively. Finally, the ΔLF2 strain was created by introducing a stop codon in the r_wt/B95.8 (6008) strain preventing the translation of the LF2 protein. Table S1 provides an overview of the different EBV strains.

EBV open reading frames (ORFs), EBV LF2, encoding a tegument protein, was identified as an inhibitor of IRF7 dimerization (14). BZLF1 also interferes with dimerization of IRF7 (15) and blocks STAT1 tyrosine phosphorylation (16), while BRLF1 controls both IRF3 and IRF7 (17). The EBV kinase BGLF4 impedes IRF3 activity through direct interactions, consequently attenuating type I IFN signaling (18). Other viral proteins, such as BGLF5 (19), inhibit production of TLR2 and TLR9.

In this study, we examined the relationship between EBV noncoding RNAs and activation of IFN response pathways. Here, we document that the EBV-encoded miRNAs contribute to the regulation of type I IFN response upon EBV infection, whereas EBERs and LF2 have a negligible effect in infected human primary B cells. We identified several BART miRNAs that regulate genes involved in the IFN secretion and IFN response pathway. The presence of viral DNA was essential to induce IFN-α secretion during EBV infection in a TLR9-dependent manner in peripheral blood mononuclear cells (PBMCs). In a newly established gp350-BlaM fusion assay, we verified that EBV virions enter a subset of pDCs and determined that these infected pDCs are the primary producers of type I IFNs in PBMCs.

RESULTS

Cloning of a reconstituted wild-type EBV strain and mutant derivatives. To study the functions of EBV miRNAs, we constructed a recombinant EBV that expresses all viral miRNAs at their physiological levels and that can be genetically manipulated in

bacteria to generate mutant derivatives. To do so, we used the wt/B95.8 (2089) recombinant virus (Fig. 1) available in our laboratory (20). This recombinant is based on the B95-8 strain of EBV (21) into which a DNA fragment encoding a green fluorescent protein (GFP) gene (used for titration), a gene encoding resistance against hygromycin (used for selection in the EBV producer cells), a chloramphenicol acetyltransferase gene (used for selection in bacteria), and the mini-F factor replicon (enabling maintenance in bacteria) have been introduced (20). We further introduced a DNA fragment from the M-ABA field strain to restore viral genes that are deleted in EBV B95-8 (22, 23). This repaired B95-8 strain derivative, termed r_wt/B95.8 (6008) (Fig. 1) (24), encodes all known EBV miRNAs that are expressed from their genuine promoters at physiological levels. In addition, r_wt/B95.8 also carries the second copy of the lytic origin of DNA replication, *oriLyt* (25), and expresses the LF1, LF2, and LF3 viral proteins from their coding sequences, which are also absent from the genome of the B95-8 EBV strain (see Table S1 in the supplemental material).

Subsequently, we replaced the viral miRNA sequences in r_wt/B95.8 with scrambled sequences, similar to our previous approach (26), preventing the expression of all viral miRNAs. This strain is called r_ΔmiR (Fig. 1) (24).

The two viral noncoding EBERs (Epstein–Barr virus-encoded small RNAs) of 167 and 172 nucleotides in length have been implicated in the activation of type I IFN responses upon EBV infection in B cells (27, 28). To evaluate their effects on type I IFN activation in our infection model, we deleted their coding sequences in r_wt/B95.8 and r_ΔmiR (Fig. 1). These two strains are called ΔEBER and ΔEBER/ΔmiR, respectively (24).

Finally, we mutated the gene encoding the LF2 viral protein that has been described as a type I IFN antagonist (14). We introduced a stop codon in the coding sequence of the LF2 gene to prevent its expression in r_wt/B95.8. This EBV strain is termed ΔLF2 (Table S1).

To conclude, we present here a fully reconstituted EBV strain based on the B95-8 EBV genome. This recombinant EBV genome can be used to produce infectious virus. It can be conveniently genetically manipulated and presumably expresses all viral genes, including all miRNAs, at their physiological levels from their authentic promoters, supported by their regulatory elements. We assume that despite its chimeric composition, this new strain represents a more physiological model than the widely used B95-8 laboratory strain.

Cytokine secretion by B lymphocytes infected by EBV mutants. We subsequently sought to determine the effects of the different mutations in the reconstituted r_wt/B95.8 EBV reference strain on the secretion of cytokines released from infected human B lymphocytes. Primary human B lymphocytes were infected *in vitro* with the five virus strains described above (r_wt/B95.8; r_ΔmiR; ΔEBER; ΔEBER/ΔmiR; ΔLF2). Upon infection with every virus strain tested, B cells grew in size and started to proliferate. Five days postinfection, infected cells were counted by flow cytometry and seeded at equal densities in fresh medium. Four days later, supernatants were collected and concentrations of interleukin-12 (IL-12), IL-6, and IFN-α were measured by enzyme-linked immunosorbent assay (ELISA) (Fig. 2).

We showed previously that EBV-encoded miRNAs regulate the expression of human IL-12 (29). As shown in Fig. 2A and B, lymphocytes infected with r_ΔmiR secreted more IL-12 than cells infected with r_wt/B95.8, consistent with prior experiments using the B95-8 strain wt/B95.8 (2089) (Fig. 1) (29). The deletion of the EBERs or LF2 did not influence IL-12 secretion. Moreover, when the cells were infected with the double mutant ΔEBER/ΔmiR, IL-12 was secreted at concentrations similar to those of r_ΔmiR-infected B cells. These data confirm that the EBV-encoded miRNAs are responsible for altered IL-12 levels in newly infected B lymphocytes, while the EBERs and LF2 do not affect IL-12 production.

We have further documented that EBV-encoded miRNAs inhibit the secretion of IL-6 but not IL-10 in the B95-8 context (29). As shown in Fig. 2B, the absence of the viral miRNAs in cells infected with r_ΔmiR led to a substantial increase in IL-6 secretion

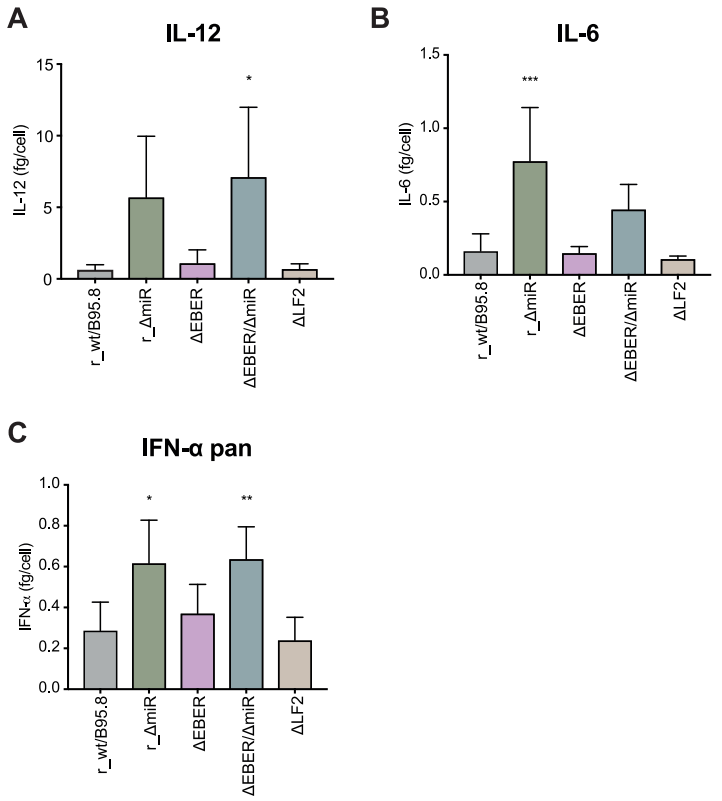

FIG 2 Cytokines secretion by infected primary B lymphocytes. Human primary B lymphocytes were infected with each of the five EBV strains at a multiplicity of infection (MOI) of 0.1 as described for Fig. 1. Five days postinfection, EBV-infected cells were counted and seeded at the same density. Four days later, the cells were counted again, the culture supernatants were collected, and cytokine levels were analyzed by ELISA. The supernatant concentrations of IL-12 (A), IL-6 (B), and IFN-α pan (C) are normalized to the final cell number and reported as fg/cell.

compared to r_wt/B95.8-infected cells. This finding demonstrates the importance of the viral miRNAs to regulate IL-6 secretion upon EBV infection. Interestingly, it has been suggested that EBER2 also plays a role in IL-6 secretion (30). We did not observe any difference in IL-6 secretion by cells infected with r_wt/B95.8 or ΔEBER, but the ΔEBER/ΔmiR-infected cells did secrete less IL-6 than the r_ΔmiR-infected cells (Fig. 2B). Results from our infection model suggest that EBERs stimulate the expression of IL-6 to some extent, but the viral miRNAs largely repress IL-6 secretion. As for IL-12 secretion, ΔLF2 behaved very similarly to r_wt/B95.8 (Fig. 2B).

We next asked whether mutations in the EBV mutant derivatives would impact the secretion of IFN-α by EBV-infected B lymphocytes. As shown in Fig. 2C, the absence of viral miRNAs led to the increased secretion of IFN-α by r_ΔmiR-infected cells compared to r_wt/B95.8-infected cells. Surprisingly, we did not observe any decrease in secreted IFN-α when comparing ΔEBER- to r_wt/B95.8-infected cells and ΔEBER/ΔmiR- to ΔmiR-infected cells. These data are puzzling, since EBERs have been reported to interact with the PRR RIG-I and act as type I IFN inducers (27, 28, 31 to 33). Additionally, ΔLF2-infected cells did not show any significant difference compared to r_wt/B95.8-infected cells despite the fact that LF2 has been shown to interact with IRF7 and block the expression of type I IFN (14). These discrepancies could be explained by differences in the experimental conditions. What we can ascertain is that, in our experiments with primary cells, the EBERs are not necessary for the expression and secretion of IFN-α by EBV-infected B lymphocytes. Moreover, independent of the presence or absence of the EBERs, the viral miRNAs significantly impact the secretion of IFN-α.

Taken together, our data indicate that EBV-encoded miRNAs prevent the secretion

of IL-12, IL-6, and IFN-α in newly infected primary human B cells. Whereas the EBERs seem to be partially responsible for the activation of IL-6, their deletion did not cause any significant difference in the secretion of IL-12, or IFN-α. We also failed to observe a contribution of LF2 to the secretion of the cytokines analyzed.

Identification of cellular transcripts regulated by EBV-encoded miRNAs. Based upon the phenotypes we observed above, we hypothesized that EBV-encoded miRNAs regulate the expression of host cellular genes involved in multiple aspects of the IFN pathways, such as PAMP sensing, production of type I IFN, and/or induction of secondary cytokine signals that encompass innate antiviral responses. To initially investigate targets of EBV miRNAs that may be involved in these pathways, we first used *in silico* prediction tools (34) to scan human 3′untranslated regions (UTRs) for the presence of canonical 7mer and 8mer miRNA seed-match sites. Candidates were cross-referenced with the literature to determine putative targets associated with PRR activation and type I IFN signaling. Among these, we identified potential binding sites for EBV miRNAs in the 3′UTRs of *DDX58/RIG-I*, *RSAD2/Viperin*, *OAS2*, and *FYN*.

To biochemically define EBV miRNA binding sites in human protein-coding transcripts, we performed PAR-CLIP experiments on latently infected DLBCL cell lines (IBL1, IBL4, and BCKN1) that express the full spectrum of EBV BHRF1 and BART miRNAs. Cells were cultured in the presence of 4-thiouridine to label RNAs as previously described (35). RISC-associated RNAs were immunopurified with antibodies to Argonaute (Ago) proteins and subjected to high-throughput sequencing. Following alignment to a human reference genome, reads were analyzed using two CLIP-seq pipelines (PARalyzer and PIPE-CLIP) to define high-resolution Ago interaction sites (36, 37). To identify host mRNAs reproducibly targeted by EBV miRNAs, we expanded our analysis to include previously published Ago PAR-CLIP data sets from EBV B95-8 and wild-type LCLs and EBV/KSHV$^+$ PEL (Table S2, Fig. S1) (35, 38–41). Derived Ago interaction sites mapping to 3′UTRs of protein-coding transcripts were scanned for canonical EBV miRNA seed matches (>=7mer1A). In total, we identified 4,010 individual genes regulated at the 3′UTR level by EBV miRNAs, with 340 genes common to all EBV-infected B-cell types investigated (DLBCLs, LCLs, PEL) (Fig. S1E).

To focus on EBV miRNA targets functionally relevant to type I IFN pathways, we interrogated Ago PAR-CLIP data using Ingenuity Pathway Analysis (IPA; Qiagen). A total of 3,976 of the 4,010 3′UTR target genes were mapped by IPA. Enriched signaling pathways included "JAK/Stat Signaling" and "Role of PKR in Interferon Induction and Antiviral Response" (Fig. S1F). Among the target genes related to IFN pathways, we identified *JAK1*, *IRF9*, *STAT1*, *IRAK2*, *IKBKB*, and interferon receptors (*IFNAR1* and *IFNAR2*). Together, these data reinforce the observation that EBV miRNAs play a major role in regulating innate immune response pathways.

EBV-encoded miRNAs regulate genes involved in the induction of type I IFN. To confirm miRNA interactions, we first selected targets with relevance to induction of type I IFN (*DDX58/RIG-I*, *RSAD2/Viperin*, *OAS2*, *FYN*, and *IRAK2*) and cloned the 3′UTRs of these genes into reporter plasmids. Reporter plasmids were cotransfected into 293T cells with or without an EBV miRNA-expressing plasmid, and luciferase expression was assessed (Fig. 3). When we observed miRNA-mediated inhibition of luciferase expression, we mutated the predicted seed sequences in the reporter plasmid and verified that the miRNA expression did not have an effect on the expression of luciferase (Fig. S2).

We initially tested miR-BART3 and miR-BART19 as regulators of the RIG-I 3′UTR (Fig. 3A). It has recently been reported that another EBV miRNA, miR-BART6, acts as a regulator of RIG-I expression and prevents the expression of type I IFN (42). Our findings confirm that EBV miRNAs control the expression of the RIG-I PRR. As the virus has evolved mechanisms to attenuate RIG-I expression, this suggests that RIG-I is involved in efficiently detecting EBV infection. Interestingly, even though the EBERs so far have been described as the primary virus moiety activating RIG-I, our data suggest that there are viral PAMPs recognized by the RIG-I helicase other than EBERs, since the

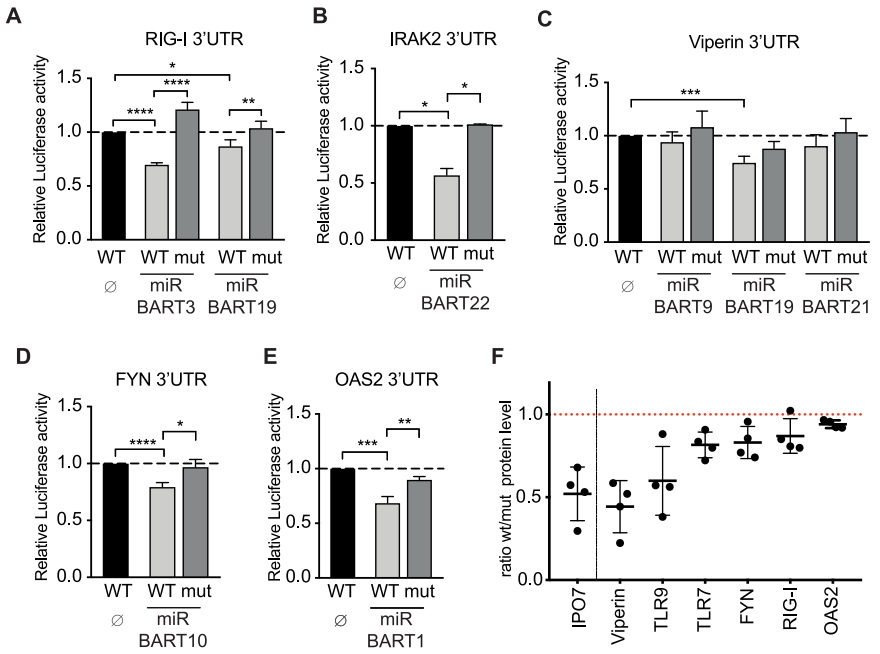

FIG 3 EBV-encoded miRNAs regulate the expression of cellular genes and proteins involved in type I IFN activation. (A to E) 293T cells were cotransfected with the indicated wild-type luciferase reporter plasmids (WT) for RIG-I/DDX58 (A), IRAK2 (B), Viperin/RSAD2 (C), FYN (D), and OAS2 (E) or reporter plasmid in which the predicted seed sequence was mutated (mut) together with or without an miRNA-encoding plasmid. The luciferase expression in these cells was assessed and normalized to lysates from cells cotransfected with the wild-type 3′-UTR reporter and empty miRNA expression plasmid (Ø). *P* values were calculated using the one-way analysis of variance (ANOVA) test. *, $P < 0.05$; **, $P < 0.01$; ***, $P < 0.001$; ****, $P < 0.0001$. (F) Human primary B lymphocytes were infected with wild-type EBV (r_wt/B95.8) or EBV devoid of its miRNAs (r_ΔmiR). Five days postinfection, EBV-infected cells were counted and seeded at the same density. Four days later, the cells were lysed and the lysates were subjected to quantitative Western blot analysis using the Western blot stain-free TGX Bio-Rad normalization approach (Bio-Rad). Blots were probed with antibodies against IPO7, Viperin/RSAD2, TLR9, TLR7, FYN, RIG-I/DDX58, and OAS2. Protein levels were quantified and used to normalize the levels of the specific protein signals. Ratios of protein levels in cells infected with wild-type virus versus cells infected with mutant virus are shown. Reported are the results of four independent biological replicates.

ΔEBER-infected cells still secrete IFN-α at levels similar to those of its wild-type predecessor, r_wt/B95.8 (Fig. 2C).

As shown in Fig. 3B to E, we found EBV-encoded miRNAs to also regulate the 3′UTRs of *IRAK2*, *RSAD2/Viperin*, *FYN*, and *OAS2*. These genes have been described as important factors for the production of type I IFN as well as activation of human pDCs. IFN-inducible *RSAD2/Viperin* promotes IFN-α secretion upon TLR7 and TLR9 activation (43), while *IRAK2* is essential for the expression of type I IFN initiated by TLR7 in pDCs (44–46). A study also showed the importance of a functional *IRAK2* for the late stage of cytokine production, including IFN-α in murine pDCs (47). Thus, modulating the expression of *IRAK2* by EBV miRNAs could contribute to regulating the release of IFN-α by pDCs via the inhibition of the TLR7 pathway.

OAS2 (2′-5′-oligoadenylate synthetase 2) is an ISG that specifically recognizes double-stranded RNA (dsRNA) structures and synthesizes 2′-5′-oligoadenylate structures that activate RNAseL. RNaseL subsequently degrades cellular and viral RNAs and, thus, inhibits translation in the infected cell. We show that miR-BART1 can regulate the 3′UTR of OAS2 in Fig. 3E; however, compared to RSAD2/Viperin, TLR9, TLR7, RIG-I, and FYN protein levels, which inversely correlated with EBV miRNA presence, OAS2 protein levels were barely upregulated in r_ΔmiR-infected cells (Fig. 3F). Together, these data show that EBV-encoded miRNAs inhibit the expression of multiple cellular factors involved in activation, expression, and secretion of type I IFN.

EBV-encoded miRNAs regulate the response to type I IFN signaling. Upon secretion, type I IFN interacts with the heterodimeric IFN-α/β receptor (IFNAR) and initiates a signaling cascade through the JAK-STAT pathway. To determine if EBV-encoded miRNAs impact type I IFN responses in addition to inhibiting IFN production, we used a reporter luciferase system whereby type I IFN was added exogenously in the presence of individual EBV miRNAs. We constructed a luciferase reporter plasmid, p6898, with the improved firefly luciferase (*luc2*) gene under the control of a chimeric promoter comprising part of the ISG Mx2 promoter and a repetition of five canonical ISREs (interferon-stimulated response element). A renilla luciferase gene under the control of the weak TK promoter was used as an internal transfection control for subsequent data normalization. We concomitantly transfected this vector into 293T cells with individual expression vectors for EBV-encoding miRNAs or an empty vector as a control. Twenty-four hours posttransfection, cells were treated with type I IFN and luciferase signals were quantified 1 day later. As a positive control, we used an miRNA expression vector for human miR-373 (Fig. 4A), which regulates the expression of *JAK1* and *IRF9* (48) and, thus, is expected to reduce the response to exogenous IFN. We also cloned and tested the IE1 gene from human cytomegalovirus (HCMV). IE1 is a very potent inhibitor of type I IFN signaling (49) and indeed efficiently suppressed luciferase expression in our assay (Fig. 4A).

Through this functional screen, we identified four EBV-encoded miRNAs that significantly attenuated the response to exogenous type I IFN (miR-BART1, miR-BART16, miR-BART22, and miR-BHRF1-2) as well as multiple other EBV miRNAs that moderately attenuated responses (Fig. 4A). miR-BART16 has recently been shown to regulate the expression of CREB-binding protein (*CBP*) and thereby inhibits the induction of ISGs (50). Targeting of the *CBP* 3′UTR was confirmed in dual-luciferase 3′UTR reporter assays (Fig. 4B).

To investigate cellular targets that are likely responsible for the phenotypes observed for the other EBV miRNAs, we examined miRNA targetome data sets (Fig. S1). Notable targets included *JAK1* and *IRF9*, which are directly involved in JAK/STAT signaling in response to type I IFN. IRF9 is part of the ISGF3 (interferon-stimulated gene factor 3), complex together with phosphorylated STAT1 and STAT2, and is required to drive the expression of ISGs upon type I IFN signaling (51). Limiting the expression of IRF9 could be a strategy employed by EBV to prevent ISGF3 complex association and the transcription of ISGs. JAK1 is a kinase, and its association with the type I IFN receptor is required to transduce the signal upon ligation of IFN on the receptor. We cloned 3′UTRs of these and other genes into dual-luciferase reporter plasmids and tested them against individual EBV miRNAs. Notably, miR-BART1 inhibited luciferase expression from the *IRF9* reporter (Fig. 4C), while miR-BART3 reduced the activity of the *JAK1* reporter (Fig. 4D). miR-BART3 had a moderate effect on luciferase expression in our IFN response assay (Fig. 4A) that could be explained by this finding. We further found that miR-BART2 regulates the *JAK2* 3′UTR, miR-BART17 regulates the *IKKB* 3′UTR, and miR-BART3 and miR-BART22 regulate *MAP3K2* (Fig. 4E to G). In our dual-luciferase reporter assays, we could further observe a suppressive effect of EBV-encoded miRNAs on reporter plasmids for *IFNAR1*, *IRF9*, *CHUK*, *ZCCHC3*, *VAV2*, *RAC1*, and *VAMP3*, which are genes with well-known functions in type I interferon signaling (Fig. S3A to H).

To confirm that EBV miRNAs indeed attenuate IFN-mediated activation of the JAK-STAT pathway, we tested a STAT-responsive luciferase reporter harboring SIS-inducible elements (SIE) in the presence of EBV miRNAs in 293T cells (Fig. 4I). Consistent with the inhibition of JAK1 and IRF9, both miR-BART1 and miR-BART3 suppressed SIE reporter activity following treatment with IFN. Quantitative reverse transcription-PCR (qRT-PCR) analysis of IFN-treated 293T cells further revealed that ISG54 and ISG56 transcript levels were reduced in the presence of miR-BART1 and miR-BART3 (Fig. S4). These data demonstrate that EBV-encoded miRNAs inhibit the expression of cellular genes involved at every step of the type I IFN pathway, including the response to type I IFN and induction of ISGs.

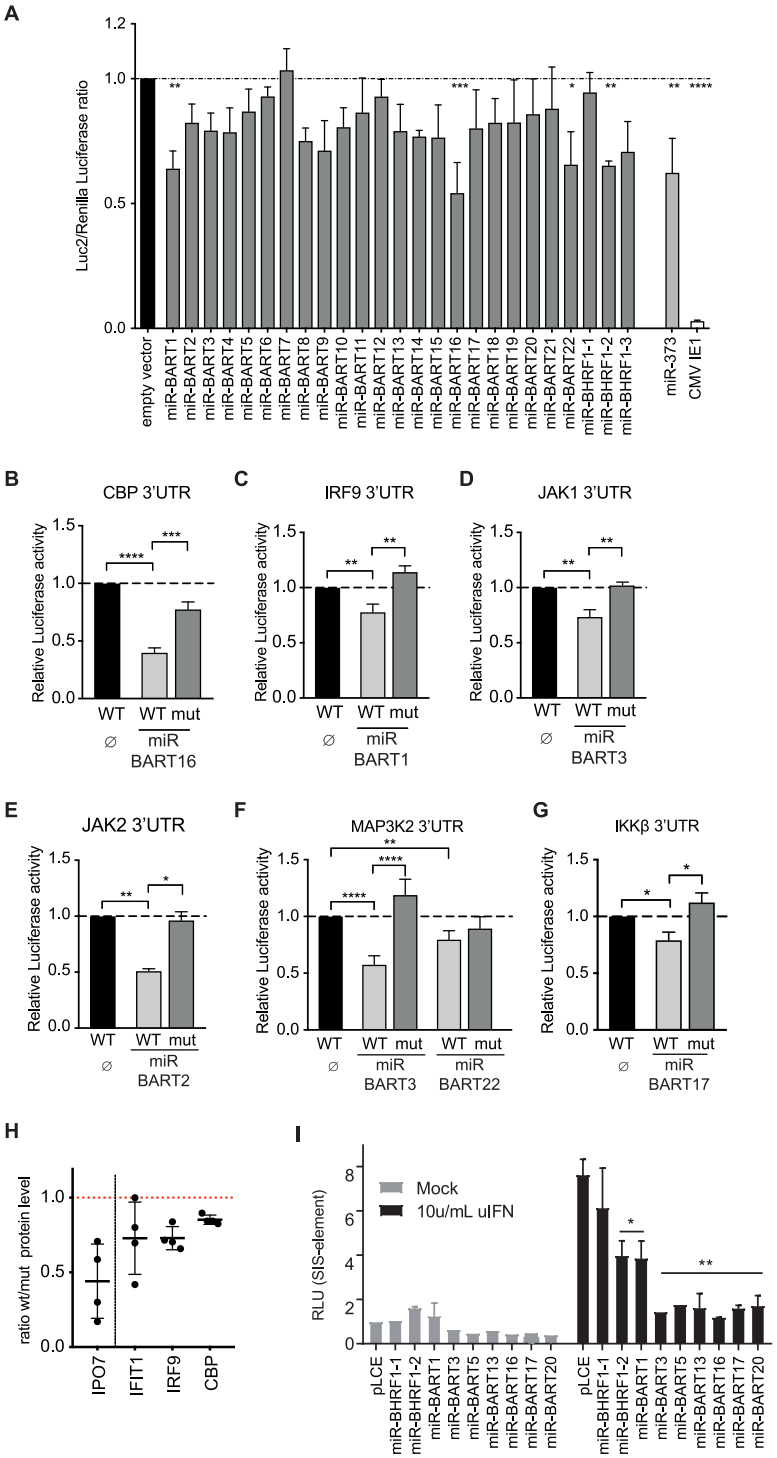

FIG 4 Interferon-stimulated genes (ISG) are regulated by EBV miRNAs. (A) 293T cells were cotransfected with individual EBV miRNA expression vectors or an empty vector as control and a reporter plasmid (p6898) containing a luc2 gene under the control of a chimeric promoter consisting of the ISG Mx2 promoter and five canonical ISREs. After 24 h, cells were treated with type I IFN and luciferase signals were measured the next day. As a control, an expression vector encoding human miRNAs (miR-373) was used (p6481). A further control was the IE1 gene from CMV, which is known to inhibit type I IFN signaling (49). *P* values were calculated by one-way ANOVA test. *, $P < 0.05$; **, $P < 0.01$; ***, $P < 0.001$; ****, $P < 0.0001$. (B to G) 293T cells were cotransfected with the indicated wild-type luciferase reporter plasmids (WT) for CBP, IRF9, JAK1, JAK2, MAPK2, and IKKβ or reporter plasmids in which the predicted seed sequences were mutated (mut) together with or without an miRNA-encoding plasmid. The luciferase expression in these cells was assessed and normalized to lysates from cells cotransfected with

(Continued on next page)

EBV-encoded miRNAs regulate the expression of proteins involved in the secretion of type I IFNs. From the identified targets of EBV-encoded viral miRNAs, we validated some at the level of protein expression. Primary human B cells were infected with the r_wt/B95.8 or r_ΔmiR EBV strains for 9 days. The cells were lysed, and the protein-adjusted cell lysates were analyzed for the expression of the indicated proteins by Western blot immunodetection. As a positive control, we monitored the expression of IPO7 (Fig. 3F and 4H), which is a published target of EBV miRNAs (52). RSAD2/Viperin, TLR9, TLR7, FYN, RIG-I/DDX58, and OAS2, which are known to be involved in type I IFN induction, are downregulated in r_wt/B95.8-infected B cells (Fig. 3F) probably directly or indirectly by EBV miRNAs. Furthermore, IFIT1, IRF9, and CBP, which are involved in the type I IFN response, are affected by EBV-encoded miRNAs (Fig. 4H).

IFN-α secretion by PBMCs and isolated pDCs infected with mutant EBV strains. We next asked whether PBMCs infected with the designed EBV mutants secrete IFN-α. We infected human PBMCs with the five EBV strains (Table S1) at three different multiplicities of infection (MOIs). Culture supernatants were collected 20 h postinfection, and secreted IFN-α was quantified by ELISA. As shown in Fig. 5A, PBMCs released IFN-α in a dose-dependent manner upon EBV infection. At the lowest MOI, r_wt/B95.8-, ΔEBER-, and ΔLF2-infected cells released a similar IFN-α concentration, while the absence of miRNAs in r_ΔmiR- and ΔEBER/ΔmiR-infected cells led to higher IFN-α secretion. At higher MOIs (0.05 and/or 0.1), the differences between the individual EBV mutants became more marked. Under these conditions, ΔEBER- and ΔLF2-infected cells released slightly more IFN-α than r_wt/B95.8-infected cells (Fig. 5A), suggesting that noncoding EBERs and the gene product of LF2 could dampen expression and/or secretion of IFN-α. Additionally, ΔEBER/ΔmiR-infected cells released more IFN-α than r_ΔmiR-infected cells, again indicating that EBERs is involved in controlling IFN-α secretion.

It has been reported that pDCs detect EBV infection and respond by releasing type I IFN (3–6). In an attempt to assess the role of viral miRNAs in the sensing of infectious EBV by pDCs, we first depleted pDCs from PBMCs. We infected pDC-depleted PBMCs with r_wt/B95.8 and r_ΔmiR using the same conditions as those described above and collected the culture supernatants 20 h postinfection. IFN-α release was quantified by ELISA. As shown in Fig. 5B, the depletion of pDCs resulted in an almost complete loss of IFN-α secretion by the remaining cells, including B lymphocytes. This finding confirms data by Severa and colleagues (6) and supports the idea that pDCs are primarily responsible for the immediate IFN-α release when PBMCs are infected with EBV (Fig. 5A). B lymphocytes barely released IFN-α immediately after PBMC infection (Fig. 5B). Moreover, in the prelatent phase, EBV-infected B lymphocytes secreted IFN-α, but at a much lower concentration (Fig. 2C) than pDCs (Fig. 5C).

We then isolated pDCs and infected the cells with the five EBV strains. As shown in Fig. 5C, r_ΔmiR-infected pDCs secreted more IFN-α than r_wt/B95.8-infected pDCs, consistent with our findings in PBMCs. ΔEBER- and ΔLF2-infected pDCs released IFN-α

FIG 4 Legend (Continued)
the wild-type 3′-UTR reporter and empty plasmid (Ø). *P* values were calculated using the one-way ANOVA test. *, $P < 0.05$; **, $P < 0.01$; ***, $P < 0.001$; ****, $P < 0.0001$. (H) Human primary B lymphocytes were infected with wild-type EBV (r_wt/B95.8) or EBV devoid of its miRNAs (r_ΔmiR). Five days postinfection, the transformed EBV-infected cells were counted and seeded at the same density. Four days later, the cells were lysed and the lysates were subjected to quantitative Western blot analysis using the Western blot stain-free TGX Bio-Rad normalization approach (Bio-Rad) and antibodies against IPO7, IFIT1, IRF9, and CBP. The applied protein amounts were analyzed and used to normalize the levels of the specific protein signals. The ratios of protein levels of cells infected with wild-type virus versus cells infected with mutant virus are shown. The figure summarizes the results of four independent replicates. (I) HEK293T cells were cotransfected with a pLCE-based EBV miRNA expression vector, a SIS-inducible element (SIE) responsive firefly luciferase reporter, and a pRL-SV40 renilla luciferase reporter as an internal control. Forty-eight hours after transfection, cells were either mock treated or treated with 10 U per ml universal type I interferon (uIFN) for 6 h and analyzed for luciferase activity. Values are normalized to mock-treated cells and reported relative to the pLCE control. Shown are the averages from three to four independent experiments performed in triplicate. Data were analyzed using Student's *t* test. *, $P < 0.05$; **, $P < 0.02$.

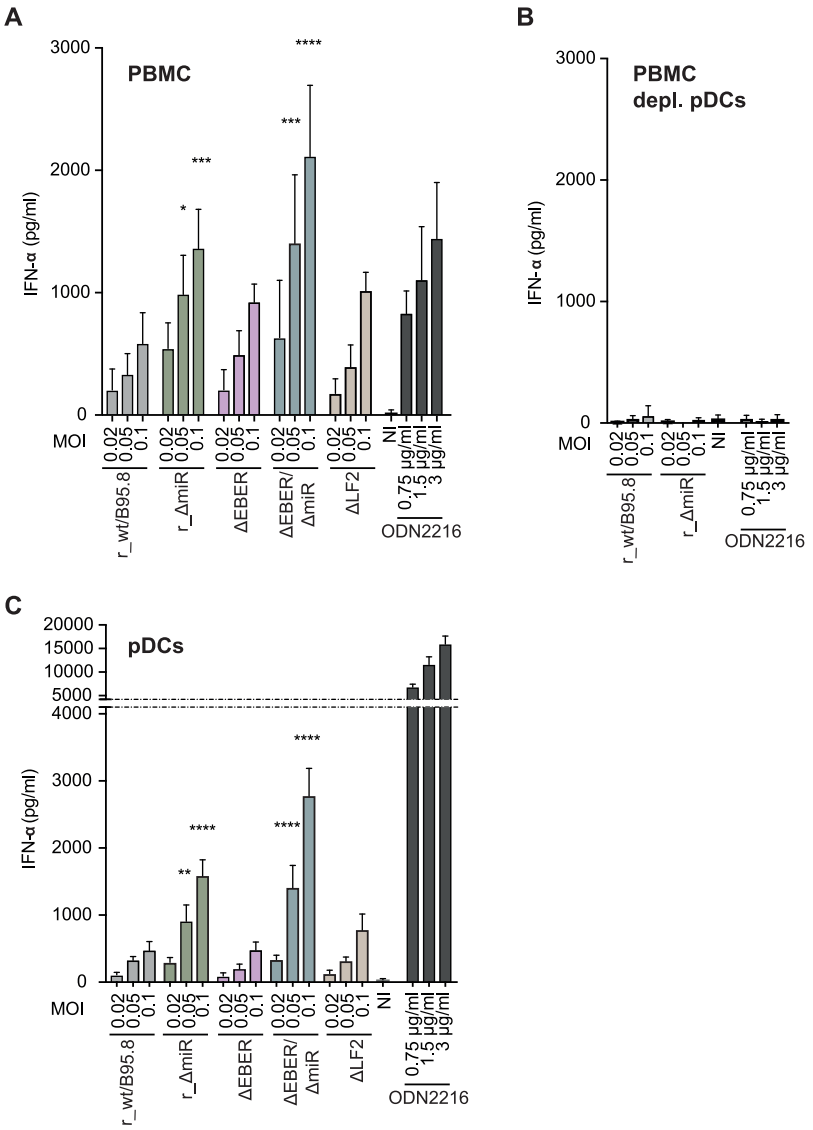

FIG 5 Plasmacytoid dendritic cells (pDCs) sense EBV infection and respond by secreting IFN-α. (A) PBMCs were infected with the five EBV strains described for Fig. 1 and listed in Table S1. The culture supernatants were collected 20 h postinfection, and IFN-α concentrations were quantified by ELISA. *P* values were calculated using the one-way ANOVA test. *, $P < 0.05$; ***, $P < 0.001$; ****, $P < 0.0001$. (B) pDCs were depleted from PBMCs using anti-CD304-coupled microbeads. The pDC-depleted PBMCs were infected with r_wt/B95.8 and r_ΔmiR using the same conditions as those for panel A, and IFN-α concentrations were determined by ELISA. (C) pDCs were isolated from buffy coats by negative selection and infected with the five EBV strains described for Fig. 1. Cell culture supernatants were collected 20 h postinfection, and IFN-α concentrations were determined by ELISA. *P* values were calculated using the one-way ANOVA test. **, $P < 0.01$; ****, $P < 0.0001$. Reported are the results of four independent biological replicates. ODN2216 is a TRL-9 agonist that was used a positive control.

similarly to r_wt/B95.8-infected cells, whereas ΔEBER/ΔmiR-infected pDCs again released the largest amount of IFN-α, suggesting that EBERs and viral miRNAs even work collaboratively and reduce the activation of the type I IFN pathway. The absence of LF2 did not seem to cause a marked effect on the secretion of IFN-α by pDCs.

Thus far, our experiments suggest that EBV miRNAs are directly involved in the regulation of type I IFN responses, especially in regulating gene expression of different pathway components. The overall impact of EBV miRNAs on direct IFN-α release by pDCs appears to be moderate, suggesting that EBV miRNAs act to reduce amplification of the IFN response in the context of PBMCs.

IFN-α release by EBV-infected cells is triggered by viral DNA and depends on TLR9 signaling. We identified pDCs as the main producers of IFN-α upon EBV infection, which is in line with published literature (1, 5, 6). As described previously, pDCs express TLR7 and TLR9, which sense viral RNA and DNA, respectively, for secreting type I IFNs (53, 54). These TLRs are found in the endosomal compartment and seem to be shifting between endosomes and lysosomes (55). We wanted to analyze if viral DNA is necessary and sufficient for the secretion of IFN-α by PBMCs upon EBV infection. EBV DNA is very rich in CpG dinucleotides, which are nonmethylated in virions (Fig. S3 in reference 78). Similar to bacterial DNA, unmethylated virion DNA is an ideal pattern for recognition by TLR9.

To this end, we infected PBMCs with the r_ΔmiR EBV strain or incubated the cells with virus-like particles (VLPs), which are free of viral DNA (56). Doses of r_ΔmiR EBV and VLPs were adjusted as described in Materials and Methods. Twenty hours postinfection, supernatants were collected and levels of IFN-α were measured. As expected, infection with r_ΔmiR led to a dose-dependent secretion of type I IFN, but PBMCs treated with VLPs did not secrete detectable levels of IFN-α (Fig. 6A, Fig. S5). To confirm that the presentation and sensing of viral DNA by pDCs is important for type I IFN release after EBV infection, we treated EBV-infected PBMCs with chloroquine. Chloroquine is an inhibitor of lysosomal functions and blocks the activation of endosomal TLRs, including TLR7 and TLR9. Chloroquine treatment of EBV-infected PBMCs led to a complete block of IFN-α release compared with PBMCs infected with EBV in the absence of the lysosome inhibitor (Fig. 6B).

The synthetic oligonucleotide deoxyribonucleotide ODN2088 is an antagonist that inhibits the TLR7/8/9-mediated responses in cells. The corresponding oligonucleotide ODN2087 is a TLR7/8 antagonist but also acts as a TLR9 antagonist control, as it has no effect on TLR9 signaling. To find out whether the IFN secretion in EBV-infected PBMCs is dependent on TLR9 as a sensor for unmethylated CpG-DNA, we infected human PBMCs with EBV r_ΔmiR in the presence of the TLR9 inhibitor ODN2088 or its ODN2087 control oligonucleotide. The inhibition of TLR9 nearly completely blocked the IFN release of EBV-infected PBMCs (Fig. 6C). When the EBV-infected PBMCs were treated with ODN2087 control, a slight drop in IFN-α levels compared to the untreated cells was noticed (Fig. 6C).

Together, these results demonstrate that IFN-α release during EBV infection of PBMCs depends on viral DNA and its detection by TLR9.

EBV-infected pDCs are the main producers of IFN-α. As shown above, type I IFN released immediately after EBV infection of PBMCs almost exclusively originates from pDCs. Our data, shown in Fig. 5, suggest that viral miRNAs and probably also the two noncoding EBERs modulate the release of IFN-α. Both classes of RNAs are contained in the tegument (i.e., the space between envelope and capsid) in EBV virions and can be delivered to EBV target cells (57–59). IFN-α release by pDCs implies that these cells endocytose EBV particles as B cells do. For pDCs to sense virion DNA and present it to the TLR9 PRR it is mandatory that EBV particles release their virion DNA, probably when endosomes reach the degradative lysosome. In this scenario, it is unclear how viral miRNAs contained in the tegument might modulate the type I IFN response unless they can be delivered into the cytoplasm of pDCs (or any other cell type where they act in conjunction with the RNA-induced silencing complex) prior to lysosomal degradation. Therefore, we asked if EBV can infect pDCs, as has been claimed previously (6), and developed an assay to determine the cell types with which EBV particles fuse to deliver their cargo into the cytoplasm.

We turned to wt/B95.8 (2089) producer cells (20) (Fig. 1), as they release very large amounts of infectious EBV upon lytic induction. We transfected the EBV 2089 producer cells with BZLF1 and BALF4 expression plasmids (to induce optimal virus synthesis) (25, 60) together with a plasmid (p7180) that expresses a carboxy-terminal fusion of the gp350 glycoprotein with a codon-optimized bacterial ß-lactamase gene. The chimeric protein, termed gp350:BlaM, was readily incorporated into infectious virions (data not shown), similar to HIV particles that contain a chimeric β-lactamase-Vpr protein (BlaM-

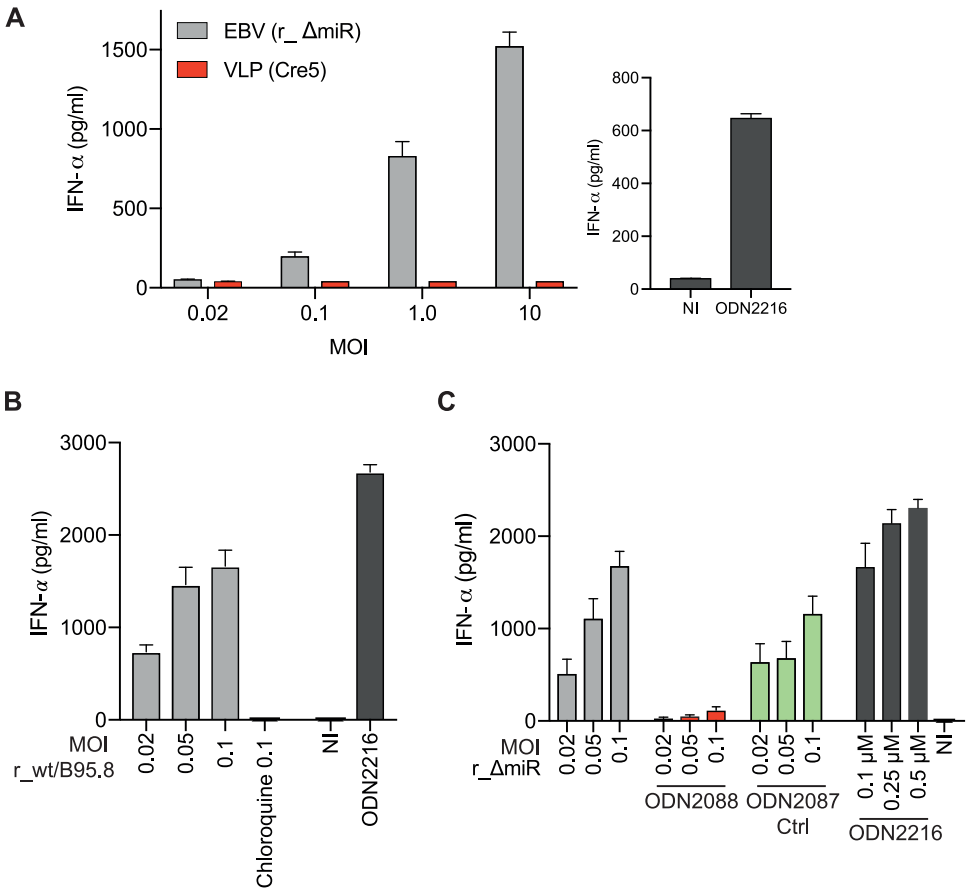

FIG 6 EBV-induced IFN-α release by PBMCs depends on viral DNA and TLR9 signaling. (A) PBMCs were infected with r_ΔmiR EBV or with virus-like particles (VLP Cre5), which do not contain viral DNA. Noninfected (NI) cells and cells treated with the TRL9 agonist ODN2216 served as negative and positive controls, respectively. The culture supernatants were collected 20 h postinfection, and the IFN-α levels were quantitated by ELISA. Means and standard deviations from three to four biological replicates are shown. (B) PBMCs were infected with EBV r_wt/B95.8 at different MOIs as indicated, with or without treatment with 100 μM chloroquine. The culture supernatants were collected 20 h postinfection, and the IFN-α levels were quantitated by ELISA. (C) PBMCs were infected with EBV r_ΔmiR using different MOIs as indicated. The cells were left untreated or were treated with 0.25 μM TLR9 antagonist ODN2088 or 0.25 μM ODN2088 control oligonucleotide, termed ODN2087. ODN2087 acts as a TLR9 antagonist control. Cells treated with different concentrations of the TRL9 agonist ODN2216 served as positive controls, and noninfected (NI) cells act as a background control. The culture supernatants were collected 20 h postinfection, and the IFN-α levels were quantitated by ELISA. Reported are the results of four independent biological replicates. ODN2216 is a TRL-9 agonist that was used a positive control.

Vpr). Upon infection, the chimeric protein is delivered into the cytoplasm of HIV target cells as a result of virion fusion (61–63).

We generated wt/B95.8 (2089) virus stocks with gp350:BlaM protein and subsequently infected PBMCs, as illustrated in Fig. 7A, for 4 h. The cells then were loaded with a cell-permeable substrate CCF4-AM and analyzed by flow cytometry. The substrate CCF4-AM is composed of a hydroxycoumarin donor conjugated to a fluorescein acceptor via a β-lactam ring (63). When target cells are infected with gp350:BlaM-assembled EBV and β-lactamase reaches the cytoplasm, the enzyme cleaves the β-lactam ring of the CCF4-AM substrate. Cleavage causes a shift of the emission wavelength from 520 nm (green) to 447 nm (blue), which can be easily detected by flow cytometry (Fig. 7A, upper).

To analyze if EBV can fuse with pDCs (i.e., infect them), we isolated pDCs from PBMCs and incubated them for 4 h with virus stocks of gp350:BlaM-assembled EBV wt/B95.8 (2089) or with EBV wt/B95.8 (2089) lacking gp350:BlaM. As an additional negative

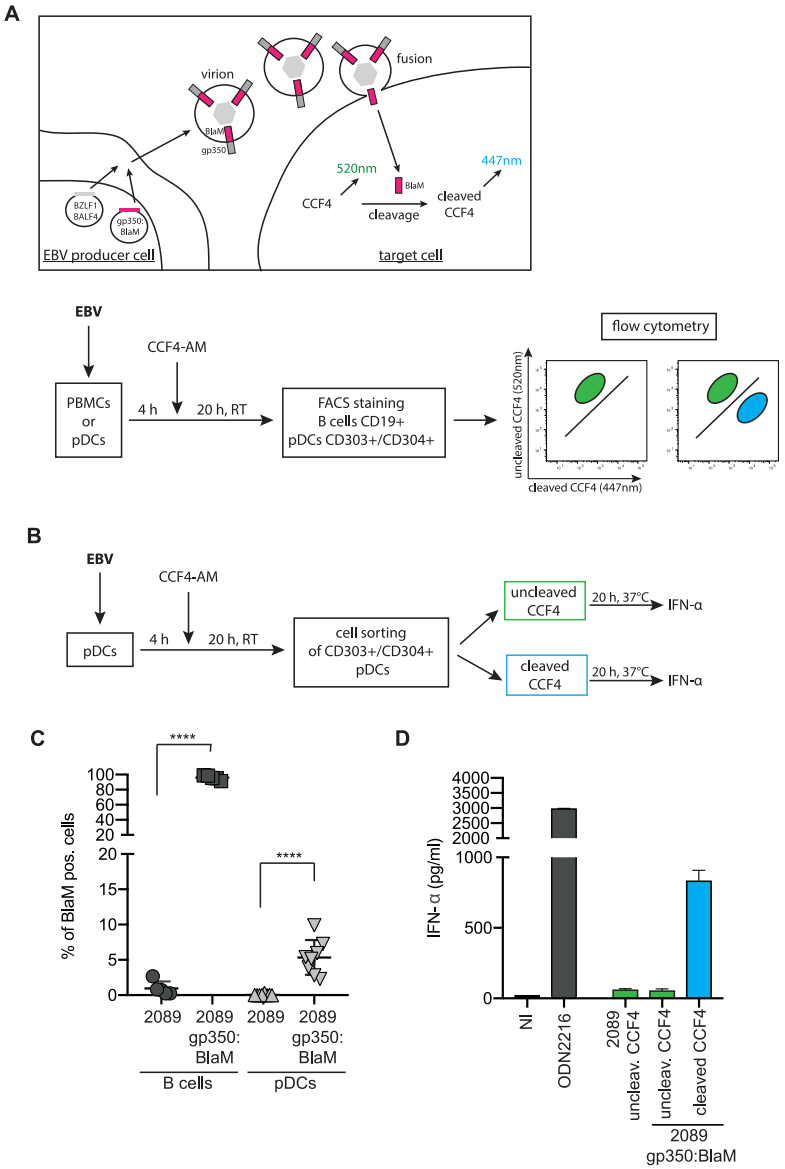

FIG 7 EBV infects a fraction of pDCs, which are the main producer of IFN-α. (A) Schematic overview of the EBV virion-based β-lactamase (BlaM) fusion assay. Expression plasmids encoding BZLF1, BALF4, and the gp350:β-lactamase (BlaM) fusion protein were cotransfected into EBV producer cells (HEK293 wt/B95.8 [2089]; Table S1). Target cells were infected with the gp350:BlaM assembled virions for 4 h and were subsequently loaded with the CCF4-AM substrate. If β-lactamase reaches the cytoplasm of the target cells, it cleaves the β-lactam ring of CCF4, which leads to a detectable shift in emission wavelength from 520 nm to 447 nm. Below, a schematic workflow of the steps of the experiment performed in panel C is shown. PBMCs were prepared from human buffy coats, and pDCs were isolated via negative selection. PBMCs and pDCs were infected with gp350:BlaM-assembled wt/B95.8 (2089) EBV at an MOI of 1. As negative controls, the cells were infected with equivalent doses of unmodified wt/B95.8 (2089) EBV. All cells were cultivated for 4 h before they were loaded with CCF4-AM and incubated at room temperature for 20 h. In the case of PBMCs, the cells were stained for B cells using a CD19 antibody, and in the case of isolated pDCs, the cells were stained with two CD303- and CD304-specific antibodies. The percentage of B cells and pDCs with green (uncleaved CCF4 substrate) and blue (cleaved CCF4 substrate) fluorescence was determined using flow cytometry. (B) Schematic representation of the steps of the experiment performed in panel D. pDCs were isolated via negative selection out of PBMCs gained from buffy coats. pDCs were treated with EBV wt/B95.8 (2089) or EBV wt/B95.8 (2089) gp350:BlaM for 4 h. Cells were washed and loaded with CCF4-AM at room temperature for 20 h. The pDCs were sorted for green and blue cell populations, and the same cell numbers were plated on 96-well cluster plates. The cells were incubated at 37°C for 20 h, and the supernatants were collected. The IFN-α levels were quantified by ELISA. (C) Results of experiments with B cells and pDCs as detailed for panel A. The *y* axis shows the fraction of cells with blue fluorescence after cleavage of CCF4. Controls are cells infected with unmodified wt/B95.8 (2089)

(Continued on next page)

control, we left the cells uninfected. As a positive control, we infected primary B lymphocytes, because they are the main target cells of EBV. After incubating the cells for 4 h with the two virus stocks and control samples, the cells were washed, loaded with the β-lactamase substrate CCF4-AM overnight at room temperature, and analyzed by flow cytometry (Fig. 7A, lower). When gp350:BlaM-assembled EBV successfully infects cells, β-lactamase cleaves the CCF4-AM substrate in the cytoplasm, resulting in a shift from green to blue fluorescence.

The main target cells of EBV are B lymphocytes. As expected, almost all B cells in PBMCs turned blue after infection with gp350:BlaM-assembled wt/B95.8 (2089) (Fig. 7C). PBMCs infected with EBV lacking gp350:BlaM, uninfected cells, or cells treated with gp350:BlaM-assembled EVs (which act as a negative control) did not contain any cells with blue fluorescence (Fig. S6, upper). To investigate whether EBV can also infect pDCs, we isolated pDCs from PBMCs using a negative selection protocol and repeated the BlaM fusion assay. pDCs infected with gp350:BlaM-assembled EBV showed approximately 5% of cells with blue fluorescence, indicating that a small fraction of pDC fuses with EBV virions (Fig. 7C, Fig. S6, lower). pDCs incubated with EVs assembled with gp350:BlaM or incubated with EBV lacking gp350:BlaM did not reveal a shift from green to blue cell fluorescence, indicating that the novel assay reflects true fusion mediated by infection with EBV (Fig. S6). Our newly established EBV BlaM fusion assay documents that EBV can infect pDCs, although at a rather low level compared with the virus's cognate B cells.

Finally, we asked whether the pDCs belonging to the small fraction that EBV infects are the main responders and, therefore, main releasers of type I IFN upon viral uptake and fusion. We infected pDCs enriched from PBMCs with gp350:BlaM-assembled wt/B95.8 (2089) EBV for 4 h, loaded the cells with CCF4-AM, and sorted them for green (noninfected) or blue (infected with gp350:BlaM-assembled EBV) populations. Identical numbers of sorted green or blue cells were plated in 96-well cluster plates, which were incubated at 37°C overnight. The next day, the supernatants were analyzed for IFN-α concentrations by ELISA. Sorted blue cells, which had been infected with gp350:BlaM-assembled EBV, showed 15-fold higher IFN-α levels than sorted noninfected cells with green fluorescence (Fig. 7D). When we infected the same number of unsorted pDCs with an identical dose of wt/B95.8 (2089) EBV, their supernatant contained low IFN-α levels comparable to the sorted, green pDCs incubated with gp350:BlaM-assembled wt/B95.8 (2089) EBV (Fig. 7D). This result was expected given the low prevalence of infected cells in unsorted pDC populations. The data indicate that those pDCs that EBV can infect respond with massive IFN-α release, whereas cells that presumably also take up EBV but degrade the incoming virions in the lysosomal pathway contribute little to IFN-α synthesis.

In summary, our experiments reveal that EBV inefficiently fuses with pDCs and that these infected pDCs are the main producers of IFN-α. The IFN-α secretion process depends on the presence of unmethylated EBV DNA, which is sensed by the PPR TLR9. Furthermore, the EBV-encoded miRNAs regulate the expression of genes involved in type I IFN secretion and genes involved in the response to type I IFNs in B cells in the prelatent phase. In pDCs cells, viral miRNAs seem to modulate cellular genes of the type I IFN pathway but, depending on the composition of the different virus preparations, only to a minor extent. Unexpectedly, our experiments indicate that the abundantly expressed noncoding small EBERs do not have a role in inducing type I IFN in either B cells or pDCs.

FIG 7 Legend (Continued)
EBV. (D) Results of experiments with isolated pDCs obtained from buffy coats as described for panel B. A total of 2×10^4 pDCs that had been sorted according to their blue fluorescence release close to 1 ng/ml IFN-α, whereas the same number of pDCs that did not show a fluorescence shift in the emission wavelength released very little IFN-α. As negative control, cells were left uninfected. As a positive control, cells that were infected but did not show a fluorescence shift were stimulated with the TLR9 agonist ODN2216.

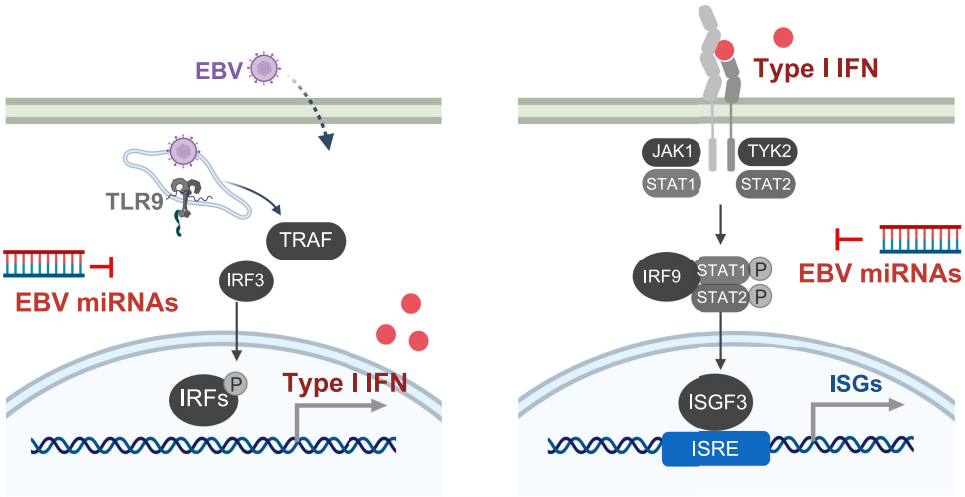

Viperin/RSAD2	miR-BART19
FYN	miR-BART10
IRAK2	miR-BART22
OAS2	miR-BART1
RIG-1/DDX58	miR-BART3, 19
RAC1	miR-BART14
VAMP3	miR-BART10
ZCCHC3	miR-BART5

IRF9	miR-BART1
JAK1	miR-BART3
IFNAR1	miR-BART2
VAV2	miR-BHRF1-3
CHUK	miR-BART7
IKBKB	miR-BART17
CBP	miR-BART16
MAP3K2	miR-BART3,22
JAK2	miR-BART2

FIG 8 Overview of the identified genes involved in innate sensing and type I IFN response regulated by EBV-encoded miRNAs. (Left) The identified target genes regulated by corresponding EBV-encoded miRNAs involved in the regulation of type I IFN production are shown. (Right) The identified target genes regulated by corresponding EBV-encoded miRNAs involved in the response to type I IFN are shown. Highlighted in red are targets for which protein expression was affected by loss of the EBV miRNAs; highlighted in blue are targets for which interactions were captured by Ago PAR-CLIP.

DISCUSSION

In this study, we examined early antiviral responses in primary B lymphocytes and pDCs infected with EBV and EBV mutants. We found that pDCs are the main source of immediate IFN-α release. In pDCs, IFN-α release was unequivocally dependent on viral DNA, which is sensed by the endosomal TLR9 receptor. In contrast to pDCs, newly infected B cells release low levels of type I IFNs later in the early, prelatent phase of infection. In infection experiments with wild-type and mutant EBVs, we determined that viral miRNAs interfere with the secretion of proinflammatory cytokines and IFN-α from newly infected B cells as well as pDCs. Bioinformatic and experimental approaches revealed that several cellular genes regulated by EBV-encoded miRNAs are involved in type I IFN secretion and response pathways (Fig. 8).

Our analysis made use of several mutant EBVs to address the contribution of the abundantly expressed small noncoding EBERs and the role of the viral LF2 gene in EBV target cells (14). Very surprisingly and contrary to previous publications, deletion of EBV EBERs had no measurable impact on IFN-α release from PBMCs, pDCs, or B lymphocytes infected with EBV. The cytoplasmic and endosomal pattern recognition receptors RIG-I and TLR3, respectively, have been reported to become activated by EBERs, inducing type I IFN release (27, 28). EBERs were also reported to confer resistance against IFN-α-induced apoptosis by binding to PKR and inhibiting its phosphorylation (64). In light of these publications, one would expect a reduced type I IFN release in infection experiments with EBER-deleted mutant EBVs, which was not the case (Fig. 5). Our experiments differed from these published studies that used established B cell lines, mostly Burkitt lymphoma cells, and experimental settings that required the ectopic expression of EBER molecules. In contrast, we infected and analyzed primary human cells and concluded our observations within a couple of days after infection. Similarly to EBV mutants devoid of EBERs, deletion of the viral gene coding for LF2

resulted in no measurable change of IFN levels compared with infections with r_wt/B95.8 EBV (Fig. 5). This result conflicts with the literature describing LF2 as a type I IFN antagonist (14). Again, experimental conditions differ substantially, as the authors relied on ectopic expression of LF2 in luciferase assays and protein-protein interactions with IRF7 in 293T cells (14).

Our findings with B-cell infection experiments (Fig. 2) provided a conundrum, as these results excluded the noncoding EBERs as viral factors that cause the release of proinflammatory cytokines (Fig. 2A and B) and IFN-α (Fig. 2C) and which the many viral miRNAs regulate. As a consequence, unknown viral PAMPs likely exist and trigger RIG-I or alternative pattern recognition receptors that presumably recognize them. Recently, several KSHV RNA fragments were identified to be sensed by RIG-I in a RNA Pol III-independent manner (65). It seems plausible that, also in the context of EBV infection, certain viral RNAs other than EBERs trigger RIG-I or other pattern recognition receptors in infected B cells. The situation in this cell type differs from experiments with PBMCs and pDCs where we could identify virion DNA as the culprit and inducer of IFN-α release (Fig. 6), confirming previous reports (3–6). Virion DNA is virtually free of methylated cytosine residues very similar to prokaryotic DNA due to a unique strategy of viral DNA replication during the productive, lytic phase of EBV infection (66).

We established a novel BlaM assay to study the potential of EBV to infect cell populations other than primary B lymphocytes. The BlaM fusion assay (Fig. 7) identified a minor fraction of EBV-infected pDCs that release much higher IFN-α levels than pDCs not detectably infected (Fig. 7D). The BlaM assay monitors the first steps in viral infection, i.e., adhesion, endosomal uptake, and the eventual fusion of cellular and viral membranes. It makes use of a transmembrane protein, which, upon fusion, translocates to the cytoplasmic compartment, where the prokaryotic ß-lactamase moiety cleaves its ingenious substrate (61, 62). Coupling the ß-lactamase reporter domain to gp350 (or another type I transmembrane protein) prevents the secretion of free enzyme and its spontaneous uptake by other cells (67). Consequently, the BlaM assay is free of erroneous background signals, supporting the identification of only positive cells in a large population of noninfected cells (Fig. 7C and D) or to detect low-level or inefficient fusion of extracellular vesicles with recipient cells (67). The BlaM assay records fusion only and is not informative as to whether viral infections are abortive or productive or lead to latent infection. As the assay does not rely on *de novo* gene expression, it can identify cells that are infected but resistant to subsequent viral gene expression and replication. These cells might still present epitopes of the incoming viral particle to immune cells, such as $CD4^+$ T cells contributing to immune responses of the infected host organism.

Previously published data show conflicting results regarding pDCs and EBV infection. Fiola et al. postulated that EBV does not establish infection in pDCs but responded to EBV particles or isolated EBV DNA, similar to our findings (3). EBV infection of pDCs and monocytes was reported to reduce biological activities of these cell types (1, 68). Li et al. further postulated that pDCs are not infected, but apoptotic and infected B cells cause the presentation of EBV antigens on major histocompatibility complex (MHC) class I molecules of DCs. Recently, it was reported that pDCs are able to undergo trogocytosis, i.e., to conjugate with antigen-presenting cells and to extract surface molecules, including MHC class I molecules, presenting them on their own cell surface. With this mechanism, noninfected pDCs could present EBV-specific epitopes on MHC class I molecules (69). On the other hand, certain isolated EBV strains efficiently infected monocytes which had been stimulated with granulocyte macrophage colony-stimulating factor (GM-CSF) and IL-4 to induce their differentiation to DCs (70). In that study, the efficiency of EBV entry into monocytes was monitored by measuring green fluorescence intensity after 48 h. In our fusion assay, we evaluated the immediate fusion of EBV with pDCs, as our incubation period was just 4 h before loading the cells with the CCF4-AM substrate, but we found only a small fraction of cells undergo fusion (Fig. 7C). In contrast, efficient infection of pDCs through viral binding to the

MHC class II molecule HLA-DR and expression of EBV genes was reported (6) together with MHC class II-mediated uptake, degradation, and subsequent activation of TLR9 followed by IFN-α secretion (5). In contrast, we did not observe the expression of viral genes (or GFP encoded by the backbone of the viral genomic DNA) in pDCs even when the cells were incubated for up to 2 days after infection with EBV (data not shown).

Our observation touches upon a key issue regarding viral miRNAs and their repressive effect on IFN-α release from pDCs, as Fig. 5C suggests: Are EBV miRNAs present in pDCs, how do they come to be present, and are they functional in pDCs? At the moment, we do not have final answers to these questions, as several possibilities must be considered. (i) EBV miRNAs could be expressed in the infected pDCs from the incoming virus. (ii) Viral miRNAs contained in the tegument compartment of virions could be delivered directly upon infection of pDCs to regulate their IFN-α release. We learned that viral miRNAs are abundant in EB virions and are readily detectable in RNA samples from infected target cells, but we do not know for sure if they are functional upon delivery (58). (iii) EBV miRNAs could also be indirectly delivered to pDCs as extracellular vesicles are shed from other infected cells present in the culture and are taken up or engulfed by the DCs. The publication by Pegtel et al. supports this idea (57), but our recent prepublished work is in stark contrast to this earlier finding (67). Clearly, the definite answer to these questions needs additional work.

Prior to our study, an accurate and direct method to monitor EBV infection of different cell populations was not available. Our newly introduced gp350-BlaM fusion assay is based on the uptake of EB virions and the fusion of their viral membrane with cellular, possibly endosomal membranes such that the content of the virion is released into the cytoplasm of EBV's host cell. Thus, our novel approach can precisely determine the fraction of cells with which EBV virions fuse within hours. Using this assay, we demonstrate that EBV virions containing gp350-BlaM fuse with the vast majority of primary B lymphocytes but only with a small fraction of pDCs (Fig. 7C). We performed dose escalation experiments but were unable to push the fraction of BlaM-positive pDCs. The highest fraction of BlaM-positive pDCs that we reached with cells from a single donor was 7.3%. Thus, it seems there is a distinct but limited population of pDCs that can pick up the virus and acts upon EBV infection by releasing type I IFN (1). These cells could be an unknown subpopulation of pDCs with uncertain cellular identity that EBV targets (Fig. 7C and D).

A closer look at the literature shows that there is a network of identified EBV-encoded miRNAs and their regulated targets. The identified target genes are mainly located in adaptive and innate immunity and immune escape mechanisms (71), which also corroborates our hypothesis that miRNAs interfere with type I IFN signaling as part of the innate immune escape during EBV infection (72–74). With our experiments shown in Fig. 3 and 4 and documented in Fig. S3 and S4, we confirmed a number of host cell transcripts targeted by viral miRNAs, but we also identified several previously unknown effectors and their cellular transcripts (Fig. 8). Already in 2017, through gene expression profiling experiments, miR-BART6-3p was reported to regulate RIG-I and IFN-β responses (42). In our study, we also confirmed that RIG-I is a target of EBV-encoded miRNAs in dual-luciferase assays and in recently infected B cells. We observed that miR-BART3 and miR-BART19 both can regulate the RIG-I 3¨UTR (Fig. 3A). These findings indicate that a combination of different miRNAs during EBV infection leads to the regulation of the same cellular gene. *CBP*, which we evaluated to be regulated by miR-BART16 (Fig. 4B), was already reported to be the target of this viral miRNA (50).

CBP, *RIG-I*, *FYN*, *IRF9*, and *JAK1* are good examples of single genes central to IFN signaling and regulated concomitantly by several EBV-encoded miRNAs (our study and reference 50). On the contrary, there are also certain genes that were reported to be regulated by EBV miRNAs, which we could not confirm in 3¨UTR luciferase reporter assays. In fact, the majority of candidates from our initial bioinformatics analysis did not pass our criteria as targets when analyzed in dual-luciferase reporter assays. For

each candidate, we cloned the 3¨UTR as well as introduced point mutations into the suspected seed match sequence to ascertain whether a functional biochemical interaction between the miRNA and its predicted mRNA target could occur. For most candidates of the screen, we were unable to confirm that the predicted miRNA interaction sites were functional. However, we found that certain cellular proteins are clearly upregulated in r_ΔmiR-infected B cells, such as TLR7 and TLR9 (Fig. 3F), but in luciferase reporter assays, we failed to identify any viral miRNAs that could regulate the 3′UTRs of these two transcripts (Fig. S7). Thus, TLR7 and TLR9 do not appear to be direct targets of EBV miRNAs, but their expression levels are certainly impacted by the presence of the viral miRNAs in EBV-infected cells.

Key experiments in this study rely on phenotypes in primary immune cells with an EBV strain and its mutant derivatives, which are based on the reconstituted wild-type EBV strain r_wt/B95.8, as shown in Fig. 1. This EBV strain carries all 25 pre-miRNAs that are processed to 44 mature viral miRNAs presumably expressed at physiological levels in EBV-infected cells. Recently, Pich et al. showed that the deletion of all miRNAs in r_ΔmiR leads to an increase in apoptosis of EBV infected primary B cells as well as a lower division index and reduced numbers of cells presented in S-phase demonstrating that EBV-encoded miRNAs are involved in the regulation of cell cycle functions (24, 26). Furthermore, studies in primary B cells showed that viral miRNAs can interfere with their immune recognition by antiviral $CD4^+$ and $CD8^+$ T cells (29, 75). Using EBV mutant derivatives (Fig. 1), we identified an additional role of viral miRNAs in governing type I IFN responses upon infection, but we were puzzled to find that the abundant EBERs do not have an apparent inducing function in this pathway. On the contrary, their deletion caused a slight but consistent increase in IFN in cells infected with the double mutant ΔEBER/ΔmiR, suggesting that the EBERs have a damping effect on the release of type I IFN in PBMCs and pDCs (Fig. 5A and C). Clearly, this finding warrants further exploration both in infection experiments and at the molecular level of type I IFN release.

MATERIALS AND METHODS

Construction of mutant EBVs. All recombinant EBVs used in this study are based on the maxi-EBV plasmid p2089, which contains the B95-8 EBV genome (20). The EBV strain B95-8 has a deletion of several pre-miRNA loci and lacks the second lytic origin of DNA replication (*oriLyt*) and several other genes, which are present in EBV field strains. As described in Pich et al. a new wild-type-like strain, based on B95-8 expressing all EBV miRNAs at the physiological level, was established. This newly generated reconstituted wild-type strain is called r_wt/B95.8 (6008) and was constructed by introducing a DNA fragment of the EBV strain M-ABA, repairing the deletion in B98-5 and the maxi-EBV plasmid p2089 (24). Furthermore, parts of the F-plasmid backbone were replaced by introducing an artificial open reading frame encoding eGFP and *pac* (*puromycin N-acetyltransferase*, conferring puromycin resistance). This new r_wt/B95.8 (6008) strain expresses all viral miRNAs at physiological levels, carries the second *oriLyt*, and expresses LF1, LF2, and LF3 viral proteins, which are absent from the B95-8 EBV genome. A second EBV strain used in this study is the r_ΔmiR (6338) strain, lacking all of the EBV-encoded pre-miRNA loci. r_ΔmiR (6338) was generated as described in detail previously (24). Furthermore, the genes of the two viral noncoding EBER RNAs were deleted in r_wt/B95.8 and r_ΔmiR to obtain mutant EBVs termed DEBER and DEBER/DmiR, respectively (Fig. 1) (24). Based on the genome of r_wt/B95.8 (6008), the viral LF2 gene was disabled by introducing a stop codon in the coding sequence of the LF2 gene. This EBV mutant was called DLF2 (Fig. 1; see also Table S1 in the supplemental material). To confirm the nucleotide sequences of all scrambled miRNA loci in r_ΔmiR, the DNA genome of a derivative of this EBV mutant strain was sequenced using Illumina's next-generation technology. To confirm the identity of ΔEBER (6431), ΔEBER/ΔmiR (6432), and ΔLF2 (6522) mutant EBVs generated and used in this and a previous study (Fig. 1 and Table S1), we used Sanger sequencing of their prokaryotic maxi-EBV DNAs to validate the relevant genomic loci modified during recombineering in *Escherichia coli* (24). Clonal HEK293 producer cell lines stably transduced with the individual maxi-EBV DNAs were checked and confirmed by Sanger sequencing of PCR-amplified template DNAs encompassing the genetically modified loci.

Cells and culture. Cells used in this study were mostly cultivated in RPMI 1640 medium supplemented with 8% fetal calf serum (FCS), 100 μg/ml streptomycin, 100 U/ml penicillin, 1 mM sodium pyruvate, 100 nM sodium selenite, and 0.43% α-thioglycerol at 37°C and 5% CO_2. HEK293 2089 cells were cultured with the addition of 100 μg/ml hygromycin and HEK293 6008, 6338, 6431, 6432, and 6522 cells with the addition of 500 ng/ml puromycin. The producer cell clone for the generation of virus-like particles (VLP Cre5; 6507) is based on the ΔmiR (4027) mutant EBV (24, 26). The ΔmiR (4027) genome DNA was further modified in *E. coli* to eliminate the packaging of its genomic viral DNA into virus particles, similar to previously published work (56). Additional modifications include a second origin of lytic DNA

replication and the replacement of the *hpt* gene with an expression cassette encoding resistance against puromycin. 293T cells for dual-luciferase reporter assays were cultured in Dulbecco's modified Eagle medium (DMEM) supplemented with 8% FCS, 100 μg/ml streptomycin, 100 U/ml penicillin, and 1 mM sodium pyruvate (Fig. 3A to E and 4B to G). HEK293T cells were maintained in high-glucose DMEM supplemented with 10% fetal bovine serum (FBS) and 1% penicillin-streptomycin-glutamine (Fig. S3D to K). DLBCL cells (IBL1, IBL4, and BCKN1) were maintained in RPMI supplemented with 10% FBS and 1% penicillin-streptomycin-glutamine.

Preparation and quantification of infectious viral stocks. HEK293 virus producer cell lines were established after transfection of the different maxi-EBV plasmids and subsequent selection with puromycin. To generate virus stocks, clonal producer cells were transfected using PEI Max with the two plasmids, p509 and p2670, to induce the lytic cycle of EBV. p509 encodes the BZLF1 gene, which triggers lytic-phase reactivation (25), and p2670 the BALF4 gene, which increases the infectivity of the recombinant EBVs (60). Three days posttransfection, supernatants were collected and centrifuged for 10 min at 1,200 rpm and 10 min at 4,000 rpm to remove cell debris. To determine the titers of the different virus stocks, we used Raji cells as described previously (76). In detail, 1×10^5 Raji cells were incubated with different amounts of virus stocks in a volume of 1 ml for 3 days at 37°C. By flow cytometry, the percentage of GFP-positive cells was determined, and the linear regression equation was calculated as described in detail in Fig. 2 of our previous work (76). To concentrate the virus, a further ultracentrifugation step with an iodixanol (OptiPrep) cushion was used. Therefore, the virus supernatants were loaded on 2 to 3 ml iodixanol (5 volumes of solution A [iodixanol] and 1 volume of solution B, containing 0.85% [wt/vol] NaCl, 60 mM HEPES, pH 7.4) and centrifuged for 2 h at 28,000 rpm at 4°C. Concentrated virus in the interphase was transferred to microfiltration tubes (Amicon Ultra-15) and centrifuged at 2,000 rpm at 4°C. Concentrated virus stocks were quantified using Raji cells as described above.

Preparation and quantification of stocks containing virus-like particles from the VLP Cre5 producer cell clone. The VLP Cre5 virus producer cell clone 6507 was derived from ΔmiR (4027) mutant EBV (24, 26), which is devoid of EBV's many miRNAs. The genome of ΔmiR (4027) was modified further to preclude the encapsidation of its genomic viral DNA into virion particles. VLP production was initiated by transient transfection of the expression plasmid p509, encoding BZLF1, similar to induction of virus producer cells described above. Three days posttransfection, supernatants were collected and centrifuged for 10 min at 1,200 rpm and 10 min at 4,000 rpm to remove cell debris. The VLP-containing supernatants were quantified using the Elijah assay, similar to the quantitation of extracellular vesicles (EVs) described below. Briefly, 2×10^5 Elijah cells (77) were incubated with different volumes of VLP-containing supernatants or with different doses of a calibrated wt/B95.8 (2089) reference EBV stock with a known virus concentration (as measured in GRU per milliliter). The Elijah cells were incubated at 4°C for 3 h on a roller mixer, subsequently washed twice with staining buffer, and resuspended in 50 μl staining buffer (phosphate-buffered saline [PBS], 0.5% bovine serum albumin [BSA], 2 mM EDTA) containing 0.2 μl of the anti-gp350 antibody 6G4 coupled to Alexa Fluor 647. Cells were incubated at 4°C for 20 min, washed with staining buffer, and analyzed by flow cytometry. The mean fluorescence intensity (MFI) values of gp350 levels were recorded, and the concentration of the EVs was calculated using the linear regression equation obtained with the aid of the reference EBV stock. Using this indirect approach, we estimated the amount of bound VLPs and determined an equivalent of GRU per milliliter of VLP stocks to ensure that their concentrations could be adjusted to GRUs of virus stocks. Based on this estimation, the measured VLPs were used at different MOIs in experiments shown in Fig. 6 and Fig. S5, together with the fully infectious r_ΔmiR (6338) EBV strain devoid of all viral miRNAs (Table S1).

Cloning and construction of luciferase reporter plasmids. Human 3′UTR sequences were amplified from genomic DNA by PCR with primers harboring Gateway-compatible extensions or restriction enzyme sites. RIG-I (DDX58), Viperin (RSAD2), IKKb (IKBKB), IRAK2, FYN, CBP, IRF9, JAK1, OAS2, JAK2, and MAP3K2 were cloned downstream of the *Renilla* luciferase (Rluc) in the modified psiCHECK-2 (Promega) plasmid p5522 using Gateway cloning technology (Fisher Scientific) (Fig. 3A to E and 4B to G). To generate other 3′UTR luciferase reporters (Fig. S3), sequences were PCR amplified from genomic DNA of EBV-infected B cells and cloned into the XhoI and NotI sites downstream of *Renilla* luciferase in the psiCheck2 dual-luciferase reporter vector containing an expanded multiple-cloning site. When achievable, the entire 3′UTR was cloned for a given target. For longer 3′UTRs, a minimum of 1 kb containing the region predicted to be targeted by each miRNA was cloned. EBV miRNA expression vectors in pLCE are previously described (41).

Luciferase reporter assays. HEK293T cells were cotransfected with 20 ng of SIS-inducible element (SIE) firefly luciferase (Fluc) reporter, 250 ng of control vector (pLCE) or EBV miRNA expression vector, and 20 ng of pRL-SV40 renilla luciferase reporter as an internal control, using Lipofectamine 2000 (Thermo Fisher) according to the manufacturer's instructions. Forty-eight hours posttransfection, cells were mock treated or treated with 10 U/ml universal type I interferon (uIFN) for 6 h and collected in 1× passive lysis buffer (Promega). Lysates were assayed for luciferase activity using the Dual-Luciferase reporter assay system (Promega) and a luminometer with dual injectors. All values are reported as relative light units (RLU) relative to luciferase internal control and normalized to the mock-treated pLCE control vector (Fig. 4F).

The 3¨UTR reporter plasmids were cotransfected into HEK293T cells using polyethyleneimine (PEI) max together with the indicated pCDH-EF1-MCS-expressing plasmids (System Biosciences) containing a cloned pre-miRNA gene of interest. Twenty-four hours posttransfection, the luciferase activity was measured using the Dual-Luciferase assay kit (Promega) and an Orion II microplate luminometer (Titertek-Berthold). The activity of Rluc was normalized to the activity of Fluc expressed by the psiCHECK-2

reporter. Site-directed mutagenesis of putative EBV miRNA seed match sites in the reporter plasmids (Fig. S2) was performed as described previously (29) (Fig. 3A to E and 4B to G, Fig. S3).

HEK293T cells plated in 96-well black-well plates were cotransfected with 20 ng of 3′UTR reporter and 250 ng of control vector (pLCE) or miRNA expression vector (41) using Lipofectamine 2000 (Thermo Fisher) according to the manufacturer's instructions. Forty-eight to 72 h posttransfection, cells were collected in 1× passive lysis buffer (Promega). Lysates were assayed for luciferase activity using the Dual-Luciferase reporter assay system (Promega) and a luminometer with dual injectors. All values are reported as RLU relative to the luciferase internal control and normalized to the pLCE control vector (Fig. S3D to K).

Generation of gp350:BlaM-assembled EVs and their quantitation using an Elijah cell binding assay. To assemble EVs with gp350:BlaM, we transfected HEK293 cells with the p7180 plasmid, which codes for a fusion of gp350 and a codon-optimized BlaM (gp350:BlaM). Three days after transfection, supernatants were harvested as described above and EVs were sedimented by ultracentrifugation at 24,000 rpm for 2 h. The EV stocks were quantified using the Elijah assay. A total of 2×10^5 Elijah cells (77) were incubated with different volumes of EVs or a calibrated wt/B95.8 (2089) reference EBV stock with a known virus concentration (as measured in GRU per milliliter). The Elijah cells were incubated at 4°C for 3 h on a roller mixer, subsequently washed twice with staining buffer (PBS, 0.5% BSA, 2 mM EDTA), and resuspended in 50 μl staining buffer containing 0.2 μl of the anti-gp350 antibody 6G4 coupled to Alexa Fluor 647. Cells were incubated at 4°C for 20 min, washed with staining buffer, and analyzed by flow cytometry. The MFI values of gp350 were recorded, and the concentration of the EVs was estimated using the linear regression equation obtained with the aid of the reference EBV stock.

Isolation of B cells from adenoids and infection. Adenoid biopsy specimens were washed with PBS and mechanically disintegrated with two sterile scalpels in a sterile petri dish. The cell suspension was filtered through a 100-μm mesh cell strainer. To obtain a maximum of single cells, this procedure was repeated. The cell suspension was brought to 50 ml with PBS, mixed, and centrifuged at 300 × *g* for 10 min. The cell pellet was resuspended in 30 ml PBS, and 0.5 ml defibrinated sheep blood for T cell rosetting was added. The cell suspension was layered onto 15 ml Ficoll Hypaque and centrifuged at 500 × *g* for 30 min. The cells were carefully collected from the interphase and transferred to a new 50-ml tube. The cells were washed two times with PBS, resuspended in 800 μl staining buffer (PBS, 0.5% BSA, 2 mM EDTA), and 70 μl CD3-allophycocyanin (APC) beads was added for 15 min at 4°C. A depletion of CD3-positive cells was done by magnetic bead sorting. The cells were washed in 10 ml staining buffer and resuspended in prewarmed medium. After counting, the cells were infected with titered virus stocks at a density of 1×10^6 cells/ml. The next day, the cells were centrifuged, resuspended in fresh medium at the same density, and cultivated. Four days later (on day five postinfection), the cells were counted using calibrated APC beads as a volume standard using a flow cytometer. The cells were incubated for 4 subsequent days at 37°C at a density of 7×10^5 cells/ml in a total volume of 2 ml in 24-well cluster plates. Afterwards, supernatants were collected for ELISA analysis.

Protein lysates from infected B cells and Western blot immunostaining. To determine the protein expression in infected B cells, B cells were isolated as described above. Infection of the isolated cells with the indicated virus stocks was performed at an initial density of 1×10^6 cells/ml. After 24 h, the cells were centrifuged and resuspended in fresh medium at the same density. Cells were incubated at 37°C for 4 or 8 additional days. Cells were washed in cold PBS and resuspended in radioimmunoprecipitation assay (RIPA) lysis buffer complemented with protease and phosphatase inhibitors. Cell lysates were frozen at −80°C. After thawing on ice, the lysates were mixed and centrifuged at 13,000 rpm for 10 min at 4°C. Supernatants were collected, and the protein amount was determined using the Bradford assay. Protein concentrations of the lysates were adjusted using RIPA lysis buffer, Lämmli buffer was added, and identical protein amounts of the different samples were loaded on TGX stain-free precast gels, purchased from Bio-Rad. After the run, the gels were activated by a 45-s UV exposure and electroblotted onto nitrocellulose membranes. The membrane was blocked and incubated with the indicated primary antibodies (Fig. 3F and 4E). The antibodies used were directed against IPO7 (SAB1402521, 1:1,000; Sigma), Viperin/RSAD2 (ab107359, 1:100; Abcam), TLR9 (sc-47723, 1:200; Santa Cruz), IFIT1 (ab70023, 1:1,000; Abcam), IRF-9 (28492, 1:1,000; Cell Signaling), TLR7 (ab124928, 1:1,000; Abcam), FYN (Fyn-59, 1:1,000; Biolegend), CBP (ab2832, 1:1,000; Abcam), RIG-I/DDX58 (AG-20B-0009, 1:1,000; Adipogen), and OAS2 (sc-374238, 1:1,000; Santa Cruz). The following secondary antibodies were used: anti-mouse horseradish peroxidase (HRP) (7076S, 1:10,000; Cell Signaling) and anti-rabbit HRP (7074S, 1:20,000; Cell Signaling). The membranes were scanned using the ChemiDoc imaging system (Bio-Rad), the images were analyzed, and the signals were quantitated after total cell protein normalization using the Image Lab 6.0.1 software (Bio-Rad).

ELISA. For detection of cytokine secretion by B cells, PBMCs, or pDCs, we used the human ELISA development kits from Mabtech for IFN-α pan (3425-1A-20), IL-12 (3455-1A-6), and IL-6 (3460-1A-6). The assays were performed as described in the manufacturer's protocol using 60 to 80 μl of cell supernatants.

Isolation and infection of PBMCs and pDCs. PBMCs were isolated from fresh whole-blood samples or buffy coats. The blood was diluted 1:3 or more in PBS, and 30 ml of the diluted blood sample was layered onto a 15-ml Ficoll Hypaque cushion in a 50-ml tube. The tubes were centrifuged at 1,850 rpm at 10°C for 30 min. PBMCs were carefully collected from the turbid interphase and were transferred to a fresh tube. Cells were washed with PBS three times at decreasing centrifugation parameters (1,600 rpm, 1,400 rpm, and 1,200 rpm for 10 min, 10°C). The cell pellet was resuspended in fresh medium, and the cells were counted. For the isolation of pDCs from PBMCs, the plasmacytoid dendritic

cell isolation kit II from Miltenyi Biotec (130-097-415) was used. The isolation of pDCs was performed as described in the manufacturer's protocol using MACS sorting with LS columns. For ELISAs, 2×10^5 PBMCs or 2×10^4 pDCs per well in 200 μl total volume were seeded in 96-well cluster plates. The cells were infected with the indicated virus strains with different MOIs, and the cells were incubated at 37°C for 20 h.

Ethics. PBMCs were obtained from volunteer blood donors. Adenoid biopsy specimens were obtained from patients from the Department of Otorhinolaryngology of the Universitätsklinikum Ludwig-Maximilian-Universität München. Biopsy specimens originated from disposed tissues from anonymous donors who underwent routine surgery.

PAR-CLIP data sets and Ingenuity Pathway Analysis. EBV B95-8 or wild-type LCLs and EBV$^+$ PEL PAR-CLIP data sets are previously described; Ago PAR-CLIP data sets for AIDS-related DLBCL cell lines (IBL1, IBL4, and BCKN1) were generated as previously described (35, 39–41). AIDS-related DLBCL cell lines were kindly provided by Ethel Cesarman (Weill Cornell Medical College) and maintained in RPMI 1640 supplemented with 20% fetal bovine serum, 2 mM L-glutamine, and antibiotics. Briefly, cells were pulsed for 18 h with 100 μM 4-thiouridine, cross-linked using UV at 365 nm, and Ago-associated RNAs were immunopurified using pan-Ago or Ago2 antibodies. Sequencing of barcoded CLIP samples was performed at the OHSU MPSSR on the Illumina HiSeq-2000 platform.

Reads were processed using the FASTX-toolkit (http://hannonlab.cshl.edu/fastx_toolkit/), aligned to the human genome (hg19) using Bowtie (-v 3, -l 12, -m 10, –best –strata), and Ago interaction sites were defined using the PARalyzer v1.5 (37) and PIPE-CLIP (36) pipelines. For PARalyzer analysis, reads are mapped to the genome, and reads that overlap by at least one nucleotide are placed into groups. Groups are then analyzed for T→C conversions, and regions with a higher likelihood of T→C conversions are posited as interaction sites so long as the minimum read depth of three reads per site is met. 3′UTR Ago interaction sites were annotated and scanned *ad hoc* for canonical seed matches (>=7mer1A) to mature EBV miRNAs.

To define major cellular pathways regulated by EBV miRNAs, we used Ingenuity Pathway Analysis (IPA) (Qiagen). A total of 3,976 human genes harboring 3′UTR miRNA interaction sites (>=7mer1A), as identified in PAR-CLIP (EBV$^+$ BC1 cells, EBV B95-8 or wild-type LCLs, and EBV$^+$ DLBCL cells), were queried. Enriched canonical pathways related to IFN-I signaling were defined by IPA, and individual pathways were selected for visual representation. Genes targeted by EBV miRNAs that modulate these enriched pathways were curated and subjected to further validation.

BlaM fusion assay. To study EBV's infectivity in different cell types, we used the BlaM fusion assay based on studies with recombinant HIV (61–63). We generated wt/B95.8 (2089) virus stocks using its producer cells, which were cotransfected with p509, p2670, and p7180 plasmid DNAs. p7180 encodes a fusion of gp350 and a codon-optimized β-lactamase. Up to 1×10^6 PBMCs or isolated pDCs were infected with wt/B95.8 (2089) assembled with gp350:BlaM or with unmodified wt/B95.8 (2089) virus as a negative control at 37°C for 4 h. Cells were washed in 200 μl CO_2 independent medium (18045-054; Gibco). The cells were loaded with CCF4-AM substrate (K1095; Thermo Fisher) in 100 μl staining solution (1 ml CO_2 independent medium, 2 μl CCF4 [K1095; Invitrogen], 8 μl solution B [K1095; Invitrogen], 10 μl Probenecid [P8761-25g; Sigma]) per well and incubated in a humidity chamber in the dark at room temperature overnight. After incubation, the cells were washed twice in fluorescence-activated cell sorting (FACS) buffer (PBS, 0.5% BSA, 2 mM EDTA) and stained with a CD19-APC antibody (302212; BioLegend) to analyze pDCs for 20 min at 4°C to analyze B cells or with two antibodies directed against CD303(BDCA2)-APC (130-097-931; Miltenyi Biotec) and CD304(BDCA4)-PE (130-112-045; Miltenyi Biotec). The cells were washed in FACS buffer (PBS, 0.5% BSA, 2 mM EDTA) and analyzed using a Fortessa flow cytometer (Becton, Dickinson). To measure the cytokine secretion of the different pDC populations, the cells were sorted using a BD FACS Aria III instrument according to the fluorescence of the CCF4-AM substrate, and identical numbers of sorted cells were seeded in 96-well cluster plates. The cells were incubated at 37°C for 20 h. The supernatants were collected, and IFN-α ELISAs were performed as described above.

Reagents. Reagents used in this study were ODN2088 (130-105-815; Miltenyi Biotech), ODN2087 Ctrl (130-105-819; Miltenyi Biotech), and chloroquine (C6628; Sigma-Aldrich).

Data availability. Raw sequencing data sets are available through NCBI SRA under BioProject no. PRJNA690834.

SUPPLEMENTAL MATERIAL

Supplemental material is available online only.

FIG S1, PDF file, 0.2 MB.

FIG S2, PDF file, 0.4 MB.

FIG S3, PDF file, 0.3 MB.

FIG S4, PDF file, 0.3 MB.

FIG S5, PDF file, 0.3 MB.

FIG S6, PDF file, 0.8 MB.

FIG S7, PDF file, 0.3 MB.

TABLE S1, DOCX file, 0.01 MB.

TABLE S2, XLSX file, 1.1 MB.

ACKNOWLEDGMENTS

We thank our colleague Nina Kirstein for her support with the many luciferase reporter assays in this study.

M.B. received an EMBO long-term fellowship from the European Molecular Biology Organization. R.L.S. and work in her laboratory are supported by NIH grants R01-AI143620 and R00-CA175181. This work was financially supported by grants from the Deutsche Forschungsgemeinschaft (grant number SFB1064/TP A13), Deutsche Krebshilfe (grant number 70112875), and German Center for Infection Research (grant number 07.814) to W.H.

M.B. and S.V. performed most of the experiments, D.P., C.G., Y.C., and D.N.F. provided additional experimental work, M.B., T.T., M.A., R.L.S., and W.H. designed the experiments and the scientific concept, and M.B., S.V., R.L.S., and W.H. wrote the paper.

REFERENCES

1. Gujer C, Murer A, Müller A, Vanoaica D, Sutter K, Jacque E, Fournier N, Kalchschmidt J, Zbinden A, Capaul R, Dzionek A, Mondon P, Dittmer U, Münz C. 2019. Plasmacytoid dendritic cells respond to Epstein-Barr virus infection with a distinct type I interferon subtype profile. Blood Adv 3:1129–1144. https://doi.org/10.1182/bloodadvances.2018025536.
2. Ungerleider N, Concha M, Lin Z, Roberts C, Wang X, Cao S, Baddoo M, Moss WN, Yu Y, Seddon M, Lehman T, Tibbetts S, Renne R, Dong Y, Flemington EK. 2018. The Epstein Barr virus circRNAome. PLoS Pathog 14:e1007206. https://doi.org/10.1371/journal.ppat.1007206.
3. Fiola S, Gosselin D, Takada K, Gosselin J. 2010. TLR9 contributes to the recognition of EBV by primary monocytes and plasmacytoid dendritic cells. J Immunol 185:3620–3631. https://doi.org/10.4049/jimmunol.0903736.
4. Lim WH, Kireta S, Russ GR, Coates PT. 2007. Human plasmacytoid dendritic cells regulate immune responses to Epstein-Barr virus (EBV) infection and delay EBV-related mortality in humanized NOD-SCID mice. Blood 109:1043–1050. https://doi.org/10.1182/blood-2005-12-024802.
5. Quan TE, Roman RM, Rudenga BJ, Holers VM, Craft JE. 2010. Epstein-Barr virus promotes interferon-alpha production by plasmacytoid dendritic cells. Arthritis Rheum 62:1693–1701. https://doi.org/10.1002/art.27408.
6. Severa M, Giacomini E, Gafa V, Anastasiadou E, Rizzo F, Corazzari M, Romagnoli A, Trivedi P, Fimia GM, Coccia EM. 2013. EBV stimulates TLR- and autophagy-dependent pathways and impairs maturation in plasmacytoid dendritic cells: implications for viral immune escape. Eur J Immunol 43:147–158. https://doi.org/10.1002/eji.201242552.
7. Takaoka A, Wang Z, Choi MK, Yanai H, Negishi H, Ban T, Lu Y, Miyagishi M, Kodama T, Honda K, Ohba Y, Taniguchi T. 2007. DAI (DLM-1/ZBP1) is a cytosolic DNA sensor and an activator of innate immune response. Nature 448:501–505. https://doi.org/10.1038/nature06013.
8. Zhang Z, Yuan B, Bao M, Lu N, Kim T, Liu YJ. 2011. The helicase DDX41 senses intracellular DNA mediated by the adaptor STING in dendritic cells. Nat Immunol 12:959–965. https://doi.org/10.1038/ni.2091.
9. Hornung V, Ablasser A, Charrel-Dennis M, Bauernfeind F, Horvath G, Caffrey DR, Latz E, Fitzgerald KA. 2009. AIM2 recognizes cytosolic dsDNA and forms a caspase-1-activating inflammasome with ASC. Nature 458:514–518. https://doi.org/10.1038/nature07725.
10. Li Y, Chen R, Zhou Q, Xu Z, Li C, Wang S, Mao A, Zhang X, He W, Shu HB. 2012. LSm14A is a processing body-associated sensor of viral nucleic acids that initiates cellular antiviral response in the early phase of viral infection. Proc Natl Acad Sci U S A 109:11770–11775. https://doi.org/10.1073/pnas.1203405109.
11. Unterholzner L, Keating SE, Baran M, Horan KA, Jensen SB, Sharma S, Sirois CM, Jin T, Latz E, Xiao TS, Fitzgerald KA, Paludan SR, Bowie AG. 2010. IFI16 is an innate immune sensor for intracellular DNA. Nat Immunol 11:997–1004. https://doi.org/10.1038/ni.1932.
12. Sun L, Wu J, Du F, Chen X, Chen ZJ. 2013. Cyclic GMP-AMP synthase is a cytosolic DNA sensor that activates the type I interferon pathway. Science 339:786–791. https://doi.org/10.1126/science.1232458.
13. Gram AM, Sun C, Landman SL, Oosenbrug T, Koppejan HJ, Kwakkenbos MJ, Hoeben RC, Paludan SR, Ressing ME. 2017. Human B cells fail to secrete type I interferons upon cytoplasmic DNA exposure. Mol Immunol 91:225–237. https://doi.org/10.1016/j.molimm.2017.08.025.
14. Wu L, Fossum E, Joo CH, Inn KS, Shin YC, Johannsen E, Hutt-Fletcher LM, Hass J, Jung JU. 2009. Epstein-Barr virus LF2: an antagonist to type I interferon. J Virol 83:1140–1146. https://doi.org/10.1128/JVI.00602-08.
15. Hahn AM, Huye LE, Ning S, Webster-Cyriaque J, Pagano JS. 2005. Interferon regulatory factor 7 is negatively regulated by the Epstein-Barr virus immediate-early gene, BZLF-1. J Virol 79:10040–10052. https://doi.org/10.1128/JVI.79.15.10040-10052.2005.
16. Morrison TE, Mauser A, Wong A, Ting JP, Kenney SC. 2001. Inhibition of IFN-gamma signaling by an Epstein-Barr virus immediate-early protein. Immunity 15:787–799. https://doi.org/10.1016/S1074-7613(01)00226-6.
17. Bentz GL, Liu R, Hahn AM, Shackelford J, Pagano JS. 2010. Epstein-Barr virus BRLF1 inhibits transcription of IRF3 and IRF7 and suppresses induction of interferon-beta. Virology 402:121–128. https://doi.org/10.1016/j.virol.2010.03.014.
18. Wang JT, Doong SL, Teng SC, Lee CP, Tsai CH, Chen MR. 2009. Epstein-Barr virus BGLF4 kinase suppresses the interferon regulatory factor 3 signaling pathway. J Virol 83:1856–1869. https://doi.org/10.1128/JVI.01099-08.
19. van Gent M, Griffin BD, Berkhoff EG, van Leeuwen D, Boer IG, Buisson M, Hartgers FC, Burmeister WP, Wiertz EJ, Ressing ME. 2011. EBV lytic-phase protein BGLF5 contributes to TLR9 downregulation during productive infection. J Immunol 186:1694–1702. https://doi.org/10.4049/jimmunol.0903120.
20. Delecluse HJ, Hilsendegen T, Pich D, Zeidler R, Hammerschmidt W. 1998. Propagation and recovery of intact, infectious Epstein-Barr virus from prokaryotic to human cells. Proc Natl Acad Sci U S A 95:8245–8250. https://doi.org/10.1073/pnas.95.14.8245.
21. Miller G, Lipman M. 1973. Release of infectious Epstein-Barr virus by transformed marmoset leukocytes. Proc Natl Acad Sci U S A 70:190–194. https://doi.org/10.1073/pnas.70.1.190.
22. Bornkamm GW, Delius H, Zimber U, Hudewentz J, Epstein MA. 1980. Comparison of Epstein-Barr virus strains of different origin by analysis of the viral DNAs. J Virol 35:603–618. https://doi.org/10.1128/JVI.35.3.603-618.1980.
23. Raab-Traub N, Dambaugh T, Kieff E. 1980. DNA of Epstein-Barr virus VIII: B95-8, the previous prototype, is an unusual deletion derivative. Cell 22:257–267. https://doi.org/10.1016/0092-8674(80)90173-7.
24. Pich D, Mrozek-Gorska P, Bouvet M, Sugimoto A, Akidil E, Grundhoff A, Hamperl S, Ling PD, Hammerschmidt W. 2019. First days in the life of naive human B lymphocytes infected with Epstein-Barr virus. mBio 10:e01723-19. https://doi.org/10.1128/mBio.01723-19.
25. Hammerschmidt W, Sugden B. 1988. Identification and characterization of oriLyt, a lytic origin of DNA replication of Epstein-Barr virus. Cell 55:427–433. https://doi.org/10.1016/0092-8674(88)90028-1.
26. Seto E, Moosmann A, Gromminger S, Walz N, Grundhoff A, Hammerschmidt W. 2010. Micro RNAs of Epstein-Barr virus promote cell cycle progression and prevent apoptosis of primary human B cells. PLoS Pathog 6:e1001063. https://doi.org/10.1371/journal.ppat.1001063.
27. Samanta M, Iwakiri D, Kanda T, Imaizumi T, Takada K. 2006. EB virus-encoded RNAs are recognized by RIG-I and activate signaling to induce type I IFN. EMBO J 25:4207–4214. https://doi.org/10.1038/sj.emboj.7601314.
28. Iwakiri D, Zhou L, Samanta M, Matsumoto M, Ebihara T, Seya T, Imai S, Fujieda M, Kawa K, Takada K. 2009. Epstein-Barr virus (EBV)-encoded small RNA is released from EBV-infected cells and activates signaling from Toll-like receptor 3. J Exp Med 206:2091–2099. https://doi.org/10.1084/jem.20081761.

29. Tagawa T, Albanese M, Bouvet M, Moosmann A, Mautner J, Heissmeyer V, Zielinski C, Lutter D, Hoser J, Hastreiter M, Hayes M, Sugden B, Hammerschmidt W. 2016. Epstein-Barr viral miRNAs inhibit antiviral CD4+ T cell responses targeting IL-12 and peptide processing. J Exp Med 213:2065–2080. https://doi.org/10.1084/jem.20160248.
30. Wu Y, Maruo S, Yajima M, Kanda T, Takada K. 2007. Epstein-Barr virus (EBV)-encoded RNA 2 (EBER2) but not EBER1 plays a critical role in EBV-induced B-cell growth transformation. J Virol 81:11236–11245. https://doi.org/10.1128/JVI.00579-07.
31. Duan Y, Li Z, Cheng S, Chen Y, Zhang L, He J, Liao Q, Yang L, Gong Z, Sun LQ. 2015. Nasopharyngeal carcinoma progression is mediated by EBER-triggered inflammation via the RIG-I pathway. Cancer Lett 361:67–74. https://doi.org/10.1016/j.canlet.2015.02.037.
32. Samanta M, Iwakiri D, Takada K. 2008. Epstein-Barr virus-encoded small RNA induces IL-10 through RIG-I-mediated IRF-3 signaling. Oncogene 27:4150–4160. https://doi.org/10.1038/onc.2008.75.
33. Iwakiri D. 2014. Epstein-Barr virus-encoded RNAs: key molecules in viral pathogenesis. Cancers 6:1615–1630. https://doi.org/10.3390/cancers6031615.
34. Garcia DM, Baek D, Shin C, Bell GW, Grimson A, Bartel DP. 2011. Weak seed-pairing stability and high target-site abundance decrease the proficiency of lsy-6 and other microRNAs. Nat Struct Mol Biol 18:1139–1146. https://doi.org/10.1038/nsmb.2115.
35. Skalsky RL, Corcoran DL, Gottwein E, Frank CL, Kang D, Hafner M, Nusbaum JD, Feederle R, Delecluse HJ, Luftig MA, Tuschl T, Ohler U, Cullen BR. 2012. The viral and cellular microRNA targetome in lymphoblastoid cell lines. PLoS Pathog 8:e1002484. https://doi.org/10.1371/journal.ppat.1002484.
36. Chen B, Yun J, Kim MS, Mendell JT, Xie Y. 2014. PIPE-CLIP: a comprehensive online tool for CLIP-seq data analysis. Genome Biol 15:R18. https://doi.org/10.1186/gb-2014-15-1-r18.
37. Corcoran DL, Georgiev S, Mukherjee N, Gottwein E, Skalsky RL, Keene JD, Ohler U. 2011. PARalyzer: definition of RNA binding sites from PAR-CLIP short-read sequence data. Genome Biol 12:R79. https://doi.org/10.1186/gb-2011-12-8-r79.
38. Al Tabaa Y, Tuaillon E, Bollore K, Foulongne V, Petitjean G, Seigneurin JM, Duperray C, Desgranges C, Vendrell JP. 2009. Functional Epstein-Barr virus reservoir in plasma cells derived from infected peripheral blood memory B cells. Blood 113:604–611. https://doi.org/10.1182/blood-2008-02-136903.
39. Gottwein E, Corcoran DL, Mukherjee N, Skalsky RL, Hafner M, Nusbaum JD, Shamulailatpam P, Love CL, Dave SS, Tuschl T, Ohler U, Cullen BR. 2011. Viral microRNA targetome of KSHV-infected primary effusion lymphoma cell lines. Cell Host Microbe 10:515–526. https://doi.org/10.1016/j.chom.2011.09.012.
40. Majoros WH, Lekprasert P, Mukherjee N, Skalsky RL, Corcoran DL, Cullen BR, Ohler U. 2013. MicroRNA target site identification by integrating sequence and binding information. Nat Methods 10:630–633. https://doi.org/10.1038/nmeth.2489.
41. Skalsky RL, Kang D, Linnstaedt SD, Cullen BR. 2014. Evolutionary conservation of primate lymphocryptovirus microRNA targets. J Virol 88:1617–1635. https://doi.org/10.1128/JVI.02071-13.
42. Lu Y, Qin Z, Wang J, Zheng X, Lu J, Zhang X, Wei L, Peng Q, Zheng Y, Ou C, Ye Q, Xiong W, Li G, Fu Y, Yan Q, Ma J. 2017. Epstein-Barr Virus miR-BART6-3p Inhibits the RIG-I Pathway. J Innate Immun 9:574–586. https://doi.org/10.1159/000479749.
43. Saitoh T, Satoh T, Yamamoto N, Uematsu S, Takeuchi O, Kawai T, Akira S. 2011. Antiviral protein Viperin promotes Toll-like receptor 7- and Toll-like receptor 9-mediated type I interferon production in plasmacytoid dendritic cells. Immunity 34:352–363. https://doi.org/10.1016/j.immuni.2011.03.010.
44. Flannery SM, Keating SE, Szymak J, Bowie AG. 2011. Human interleukin-1 receptor-associated kinase-2 is essential for Toll-like receptor-mediated transcriptional and post-transcriptional regulation of tumor necrosis factor alpha. J Biol Chem 286:23688–23697. https://doi.org/10.1074/jbc.M111.248351.
45. Kawagoe T, Sato S, Matsushita K, Kato H, Matsui K, Kumagai Y, Saitoh T, Kawai T, Takeuchi O, Akira S. 2008. Sequential control of Toll-like receptor-dependent responses by IRAK1 and IRAK2. Nat Immunol 9:684–691. https://doi.org/10.1038/ni.1606.
46. Wang H, El Maadidi S, Fischer J, Grabski E, Dickhöfer S, Klimosch S, Flannery SM, Filomena A, Wolz OO, Schneiderhan-Marra N, Löffler MW, Wiese M, Pichulik T, Müllhaupt B, Semela D, Dufour JF, Bochud PY, Bowie AG, Kalinke U, Berg T, Weber AN, East-German and Swiss Hepatitis C Virus Study Groups. 2015. A frequent hypofunctional IRAK2 variant is associated with reduced spontaneous hepatitis C virus clearance. Hepatology 62:1375–1387. https://doi.org/10.1002/hep.28105.
47. Pauls E, Nanda SK, Smith H, Toth R, Arthur JSC, Cohen P. 2013. Two phases of inflammatory mediator production defined by the study of IRAK2 and IRAK1 knock-in mice. J Immunol 191:2717–2730. https://doi.org/10.4049/jimmunol.1203268.
48. Mukherjee A, Di Bisceglie AM, Ray RB. 2015. Hepatitis C virus-mediated enhancement of microRNA miR-373 impairs the JAK/STAT signaling pathway. J Virol 89:3356–3365. https://doi.org/10.1128/JVI.03085-14.
49. Piganis RA, De Weerd NA, Gould JA, Schindler CW, Mansell A, Nicholson SE, Hertzog PJ. 2011. Suppressor of cytokine signaling (SOCS) 1 inhibits type I interferon (IFN) signaling via the interferon alpha receptor (IFNAR1)-associated tyrosine kinase Tyk2. J Biol Chem 286:33811–33818. https://doi.org/10.1074/jbc.M111.270207.
50. Hooykaas MJG, van Gent M, Soppe JA, Kruse E, Boer IGJ, van Leenen D, Groot Koerkamp MJA, Holstege FCP, Ressing ME, Wiertz EJHJ, Lebbink RJ. 2017. EBV microRNA BART16 suppresses type I IFN signaling. J Immunol 198:4062–4073. https://doi.org/10.4049/jimmunol.1501605.
51. Qureshi SA, Salditt-Georgieff M, Darnell JE. 1995. Tyrosine-phosphorylated Stat1 and Stat2 plus a 48-kDa protein all contact DNA in forming interferon-stimulated-gene factor 3. Proc Natl Acad Sci U S A 92:3829–3833. https://doi.org/10.1073/pnas.92.9.3829.
52. Dölken L, Malterer G, Erhard F, Kothe S, Friedel CC, Suffert G, Marcinowski L, Motsch N, Barth S, Beitzinger M, Lieber D, Bailer SM, Hoffmann R, Ruzsics Z, Kremmer E, Pfeffer S, Zimmer R, Koszinowski UH, Grasser F, Meister G, Haas J. 2010. Systematic analysis of viral and cellular microRNA targets in cells latently infected with human gamma-herpesviruses by RISC immunoprecipitation assay. Cell Host Microbe 7:324–334. https://doi.org/10.1016/j.chom.2010.03.008.
53. Colonna M, Trinchieri G, Liu YJ. 2004. Plasmacytoid dendritic cells in immunity. Nat Immunol 5:1219–1226. https://doi.org/10.1038/ni1141.
54. Reizis B. 2019. Plasmacytoid dendritic cells: development, regulation, and function. Immunity 50:37–50. https://doi.org/10.1016/j.immuni.2018.12.027.
55. Ahmad-Nejad P, Häcker H, Rutz M, Bauer S, Vabulas RM, Wagner H. 2002. Bacterial CpG-DNA and lipopolysaccharides activate Toll-like receptors at distinct cellular compartments. Eur J Immunol 32:1958–1968. https://doi.org/10.1002/1521-4141(200207)32:7<1958::AID-IMMU1958>3.0.CO;2-U.
56. Hettich E, Janz A, Zeidler R, Pich D, Hellebrand E, Weissflog B, Moosmann A, Hammerschmidt W. 2006. Genetic design of an optimized packaging cell line for gene vectors transducing human B cells. Gene Ther 13:844–856. https://doi.org/10.1038/sj.gt.3302714.
57. Pegtel DM, Cosmopoulos K, Thorley-Lawson DA, van Eijndhoven MA, Hopmans ES, Lindenberg JL, de Gruijl TD, Wurdinger T, Middeldorp JM. 2010. Functional delivery of viral miRNAs via exosomes. Proc Natl Acad Sci U S A 107:6328–6333. https://doi.org/10.1073/pnas.0914843107.
58. Jochum S, Ruiss R, Moosmann A, Hammerschmidt W, Zeidler R. 2012. RNAs in Epstein-Barr virions control early steps of infection. Proc Natl Acad Sci U S A 109:E1396–E1404. https://doi.org/10.1073/pnas.1115906109.
59. Baglio SR, van Eijndhoven MA, Koppers-Lalic D, Berenguer J, Lougheed SM, Gibbs S, Léveillé N, Rinkel RN, Hopmans ES, Swaminathan S, Verkuijlen SA, Scheffer GL, van Kuppeveld FJ, de Gruijl TD, Bultink IE, Jordanova ES, Hackenberg M, Piersma SR, Knol JC, Voskuyl AE, Wurdinger T, Jiménez CR, Middeldorp JM, Pegtel DM. 2016. Sensing of latent EBV infection through exosomal transfer of 5′pppRNA. Proc Natl Acad Sci U S A 113:E587–E596. https://doi.org/10.1073/pnas.1518130113.
60. Neuhierl B, Feederle R, Hammerschmidt W, Delecluse HJ. 2002. Glycoprotein gp110 of Epstein-Barr virus determines viral tropism and efficiency of infection. Proc Natl Acad Sci U S A 99:15036–15041. https://doi.org/10.1073/pnas.232381299.
61. Cavrois M, De Noronha C, Greene WC. 2002. A sensitive and specific enzyme-based assay detecting HIV-1 virion fusion in primary T lymphocytes. Nat Biotechnol 20:1151–1154. https://doi.org/10.1038/nbt745.
62. Cavrois M, Neidleman J, Greene WC. 2014. HIV-1 fusion assay. Bio Protoc 4:e1212.
63. Jones DM, Padilla-Parra S. 2016. The β-lactamase assay: harnessing a FRET biosensor to analyse viral fusion mechanisms. Sensors 16:950. https://doi.org/10.3390/s16070950.
64. Nanbo A, Inoue K, Adachi-Takasawa K, Takada K. 2002. Epstein-Barr virus RNA confers resistance to interferon-alpha-induced apoptosis in Burkitt's lymphoma. EMBO J 21:954–965. https://doi.org/10.1093/emboj/21.5.954.
65. Zhang Y, Dittmer DP, Mieczkowski PA, Host KM, Fusco WG, Duncan JA, Damania B. 2018. RIG-I detects Kaposi's sarcoma-associated herpesvirus

transcripts in a RNA polymerase III-independent manner. mBio 9:e00823-18. https://doi.org/10.1128/mBio.00823-18.
66. Buschle A, Hammerschmidt W. 2020. Epigenetic lifestyle of Epstein-Barr virus. Semin Immunopathol 42:131–142. https://doi.org/10.1007/s00281-020-00792-2.
67. Albanese M, Chen Y-FA, Hüls C, Gärtner K, Tagawa T, Mejias-Perez E, Keppler OT, Göbel C, Zeidler R, Shein M, Schütz AK, Hammerschmidt W. 2020. Micro RNAs are minor constituents of extracellular vesicles and are hardly delivered to target cells. bioRxiv https://doi.org/10.1101/2020.05.20.106393.
68. Li L, Liu D, Hutt-Fletcher L, Morgan A, Masucci MG, Levitsky V. 2002. Epstein-Barr virus inhibits the development of dendritic cells by promoting apoptosis of their monocyte precursors in the presence of granulocyte macrophage-colony-stimulating factor and interleukin-4. Blood 99:3725–3734. https://doi.org/10.1182/blood.v99.10.3725.
69. Bonaccorsi I, Morandi B, Antsiferova O, Costa G, Oliveri D, Conte R, Pezzino G, Vermiglio G, Anastasi GP, Navarra G, Münz C, Di Carlo E, Mingari MC, Ferlazzo G. 2014. Membrane transfer from tumor cells overcomes deficient phagocytic ability of plasmacytoid dendritic cells for the acquisition and presentation of tumor antigens. J Immunol 192:824–832. https://doi.org/10.4049/jimmunol.1301039.
70. Guerreiro-Cacais AO, Li L, Donati D, Bejarano MT, Morgan A, Masucci MG, Hutt-Fletcher L, Levitsky V. 2004. Capacity of Epstein-Barr virus to infect monocytes and inhibit their development into dendritic cells is affected by the cell type supporting virus replication. J Gen Virol 85:2767–2778. https://doi.org/10.1099/vir.0.80140-0.
71. Albanese M, Tagawa T, Buschle A, Hammerschmidt W. 2017. microRNAs of Epstein-Barr virus control innate and adaptive anti-viral immunity. J Virol 91:e01667-16. https://doi.org/10.1128/JVI.01667-16.
72. Li W, He C, Wu J, Yang D, Yi W. 2020. Epstein Barr virus encodes miRNAs to assist host immune escape. J Cancer 11:2091–2100. https://doi.org/10.7150/jca.42498.
73. Gallo A, Miceli V, Bulati M, Iannolo G, Contino F, Conaldi PG. 2020. Viral miRNAs as active players and participants in tumorigenesis. Cancers 12:358. https://doi.org/10.3390/cancers12020358.
74. Iizasa H, Kim H, Kartika AV, Kanehiro Y, Yoshiyama H. 2020. Role of viral and host microRNAs in immune regulation of Epstein-Barr virus-associated diseases. Front Immunol 11:367. https://doi.org/10.3389/fimmu.2020.00367.
75. Albanese M, Tagawa T, Bouvet M, Maliqi L, Lutter D, Hoser J, Hastreiter M, Hayes M, Sugden B, Martin L, Moosmann A, Hammerschmidt W. 2016. Epstein-Barr virus microRNAs reduce immune surveillance by virus-specific CD8+ T cells. Proc Natl Acad Sci U S A 113:E6467–E6475. https://doi.org/10.1073/pnas.1605884113.
76. Steinbrück L, Gustems M, Medele S, Schulz TF, Lutter D, Hammerschmidt W. 2015. K1 and K15 of Kaposi's sarcoma-associated herpesvirus are partial functional homologues of latent membrane protein 2A of Epstein-Barr virus. J Virol 89:7248–7261. https://doi.org/10.1128/JVI.00839-15.
77. Rowe M, Rooney CM, Rickinson AB, Lenoir GM, Rupani H, Moss DJ, Stein H, Epstein MA. 1985. Distinctions between endemic and sporadic forms of Epstein-Barr virus-positive Burkitt's lymphoma. Int J Cancer 35:435–441. https://doi.org/10.1002/ijc.2910350404.
78. Kalla M, Schmeinck A, Bergbauer M, Pich D, Hammerschmidt W. 2010. AP-1 homolog BZLF1 of Epstein–Barr virus has two essential functions dependent on the epigenetic state of the viral genome. Proc Natl Acad Sci U S A 107:850–855. https://doi.org/10.1073/pnas.0911948107.